

MULTIPLE-SCATTERING T -MATRIX SIMULATIONS FOR NANOPHOTONICS: SYMMETRIES AND PERIODIC LATTICES

MAREK NEČADA AND PÄIVI TÖRMÄ

Department of Applied Physics, Aalto University School of Science, P.O. Box 15100, FI-00076 Aalto, Finland

ABSTRACT. The multiple scattering method T -matrix (MSTMM) can be used to solve the electromagnetic response of systems consisting of many compact scatterers, retaining a good level of accuracy while using relatively few degrees of freedom, largely surpassing other methods in the number of scatterers it can deal with. Here we extend the method to infinite periodic structures using Ewald-type lattice summation, and we exploit the possible symmetries of the structure to further improve its efficiency, so that systems containing tens of thousands of particles can be studied with relative ease. We release a modern implementation of the method, including the theoretical improvements presented here, under GNU General Public Licence.

E-mail address: marek@necada.org, paivi.torma@aalto.fi.

2000 Mathematics Subject Classification. 78-10, 78-04, 78M16, 78A45, 65R20, 35B27.

Key words and phrases. T -matrix, multiple scattering, lattice modes, symmetry-adapted basis, metamaterials, Ewald summation.

1. INTRODUCTION

The problem of electromagnetic response of a system consisting of many relatively small, compact scatterers in various geometries, and its numerical solution, is relevant to several branches of nanophotonics. In practice, the scatterers often form some ordered structure, such as metallic or dielectric nanoparticle arrays [61, 8, 53, 22] that offer many degrees of tunability, with applications including structural color, ultra-thin lenses [21], strong coupling between light and quantum emitters [50, 40, 49], weak and strong coupling lasing and Bose-Einstein condensation [60, 11, 10, 12, 58, 41, 51, 52], magneto-optical effects [20], or sensing [25]. The number of scatterers tends to be rather large; unfortunately, the most common general approaches used in computational electrodynamics are often unsuitable for simulating systems with larger number of scatterers due to their computational complexity: differential methods such as the finite difference time domain (FDTD, [48]) method or the finite element method (FEM, [38]) include the field degrees of freedom (DoF) of the background medium (which can have very large volumes), whereas integral approaches such as the boundary element method (BEM, a.k.a the method of moments, MOM [14, 32, 43]) need much less DoF but require working with dense matrices containing couplings between each pair of DoF. Therefore, a common (frequency-domain) approach to get an approximate solution of the scattering problem for many small particles has been the coupled dipole approximation (CD) [59] where a drastic reduction of the number of DoF is achieved by approximating individual scatterers to electric dipoles (characterised by a polarisability tensor) coupled to each other through Green's functions.

CD is easy to implement and demands relatively little computational resources but suffers from at least two fundamental drawbacks. The obvious one is that the dipole approximation is too rough for particles with diameter larger than a small fraction of the wavelength, which results to quantitative errors. The other one, more subtle, manifests itself in photonic crystal-like structures used in nanophotonics: there are modes in which the particles' electric dipole moments completely vanish due to symmetry, and regardless of how small the particles are, the excitations have quadrupolar or higher-degree multipolar character. These modes, belonging to a category that is sometimes called *optical bound states in the continuum (BIC)* [15], typically appear at the band edges where interesting phenomena such as lasing or Bose-Einstein condensation have been observed [10, 37, 11, 58, 12] – and CD by definition fails to capture such modes.

The natural way to overcome both limitations of CD mentioned above is to take higher multipoles into account. Instead of a polarisability tensor, the scattering properties of an individual particle are then described with more general *transition matrix* (commonly known as *T-matrix*), and different particles' multipole excitations are coupled together via translation operators, a generalisation of the Green's functions used in CDA. This is the idea behind the *multiple-scattering T-matrix method* (MSTMM), a.k.a. *superposition T-matrix method* [27], and it has been implemented many times in the context of electromagnetics [44], but usually only as specific codes for limited subsets of problems, such as scattering by clusters of spheres, circular cylinders, or Chebyshev particles [28, 29, 57]; there also exists a code for modeling photonic slabs including 2D-periodic infinite arrays of spheres [46, 47]. Perhaps the most general MSTMM software with respect to the system

geometry has been FaSTMM [31, 30], which also a rare example is in this field of a publicly available code with a clear licence.

However, the potential of MSTMM reaches far beyond its past implementations. Here we present several enhancements to the method, which are especially useful in metamaterial and nanophotonics simulations. We extend the method on infinite periodic lattices (in all three possible dimensionalities) using Ewald-type summation techniques. This enables, among other things, to use MSTMM for fast solving of the lattice modes of such periodic systems, and comparing them to their finite counterparts with respect to electromagnetic response, which is useful to isolate the bulk and finite-size phenomena of photonic lattices. Moreover, we exploit symmetries of the system to decompose the problem into several substantially smaller ones, which provides better understanding of modes, mainly in periodic systems, and substantially reduces the demands on computational resources, hence speeding up the computations and allowing for finite size simulations of systems with particle numbers practically impossible to reliably simulate with any other method. Furthermore, the method can be combined with other integral methods, which removes the limitation to systems with compact scatterers only, and enables e.g. including a substrate [3].

The power of the method has been already demonstrated by several works where we used it to explain experimental observations: the finite lattice size effects on dipole patterns and phase profiles of the nanoparticle lattice modes in [11], symmetry and polarisation analysis of the modes at the K -point of a honeycomb nanoparticle lattice in [10], the structure of lasing modes in a Ni nanoparticle array [37] and energy spacing between the Γ -point modes in a finite lattice [51].

We hereby release our MSTMM implementation, the *QPMS Photonic Multiple Scattering* suite [36], as free software under the GNU General Public License version 3. QPMS allows for linear optics simulations of arbitrary sets of compact scatterers in isotropic media. The features include computations of electromagnetic response to external driving, the related cross sections, and finding resonances of finite structures. Moreover, it includes the improvements covered in this article, enabling to simulate even larger systems and also infinite structures with periodicity in one, two or three dimensions, which can be used e.g. for evaluating dispersions of such structures. The QPMS suite contains a core C library, Python bindings and several utilities for routine computations, such as scattering cross sections under plane wave irradiation or lattice modes of two-dimensional periodic arrays. It includes Doxygen documentation together with description of the API. It has been written with customisability and extendibility in mind, so that including e.g. alternative methods of T -matrix calculations of a single particle's matrix are as easy as possible.

The current paper is organised as follows: Section 2 provides a review of MSTMM theory for finite systems. In Section 3 we develop the theory for infinite periodic structures. In Section 4 we apply group theory on MSTMM to utilise the symmetries of the simulated system. Finally, Section 5 shows some practical results that can be obtained using QPMS.

2. FINITE SYSTEMS

The basic idea of MSTMM is quite simple: the driving electromagnetic field incident onto a scatterer is expanded into a vector spherical wavefunction (VSWF) basis in which the single scattering problem is solved, and the scattered field is then re-expanded into VSWFs centered at the other scatterers. Repeating the same procedure with all (pairs of) scatterers yields a set of linear equations, solution of which gives the coefficients of the scattered field in the VSWF bases. Once these coefficients have been found, one can evaluate various quantities related to the scattering (such as cross sections or the scattered fields) quite easily.

The expressions appearing in the re-expansions are fairly complicated, and the implementation of MSTMM is extremely error-prone also due to the various conventions used in the literature. Therefore although we do not re-derive from scratch the expressions that can be found elsewhere in literature, for reader's reference we always state them explicitly in our convention.

2.1. Single-particle scattering. In order to define the basic concepts, let us first consider the case of electromagnetic (EM) radiation scattered by a single particle. We assume that the scatterer lies inside a closed ball $\overline{B}_{R^<}(\mathbf{0})$ of radius $R^<$ and center in the origin of the coordinate system (which can be chosen that way; the natural choice of $\overline{B}_{R^<}(\mathbf{0})$ is the circumscribed ball of the scatterer) and that there exists a larger open cocentric ball $B_{R^>}(\mathbf{0})$, such that the (non-empty) spherical shell $\Theta_{R^<,R^>}(\mathbf{0}) = B_{R^>}(\mathbf{0}) \setminus \overline{B}_{R^<}(\mathbf{0})$ is filled with a homogeneous isotropic medium with relative electric permittivity $\epsilon(\mathbf{r}, \omega) = \epsilon_b(\omega)$ and magnetic permeability $\mu(\mathbf{r}, \omega) = \mu_b(\omega)$, and that the whole system is linear, i.e. the material properties of neither the medium nor the scatterer depend on field intensities. Under these assumptions, the EM fields $\Psi = \mathbf{E}, \mathbf{H}$ in $\Theta_{R^<,R^>}(\mathbf{0})$ must satisfy the homogeneous vector Helmholtz equation together with the transversality condition

$$(2.1) \quad (\nabla^2 + \kappa^2) \Psi(\mathbf{r}, \omega) = 0, \quad \nabla \cdot \Psi(\mathbf{r}, \omega) = 0$$

with wave number¹ $\kappa = \kappa(\omega) = \omega \sqrt{\mu_b(\omega)\epsilon_b(\omega)}/c_0$, as can be derived from Maxwell's equations [16].

2.1.1. Spherical waves. Equation 2.1 can be solved by separation of variables in spherical coordinates to give the solutions – the *regular* and *outgoing* vector spherical wavefunctions (VSWFs) $\mathbf{v}_{\tau lm}(\kappa \mathbf{r})$ and $\mathbf{u}_{\tau lm}(\kappa \mathbf{r})$, respectively, defined as follows:

$$(2.2) \quad \begin{aligned} \mathbf{v}_{1lm}(\kappa \mathbf{r}) &= j_l(\kappa r) \mathbf{A}_{1,l,m}(\hat{\mathbf{r}}), \\ \mathbf{v}_{2lm}(\kappa \mathbf{r}) &= \frac{1}{\kappa r} \frac{d(\kappa r j_l(\kappa r))}{d(\kappa r)} \mathbf{A}_{2,l,m}(\hat{\mathbf{r}}) + \sqrt{l(l+1)} \frac{j_l(\kappa r)}{\kappa r} \mathbf{A}_{3,l,m}(\hat{\mathbf{r}}), \end{aligned}$$

$$(2.3) \quad \begin{aligned} \mathbf{u}_{1lm}(\kappa \mathbf{r}) &= h_l^{(1)}(\kappa r) \mathbf{A}_{1,l,m}(\hat{\mathbf{r}}), \\ \mathbf{u}_{2lm}(\kappa \mathbf{r}) &= \frac{1}{\kappa r} \frac{d(\kappa r h_l^{(1)}(\kappa r))}{d(\kappa r)} \mathbf{A}_{2,l,m}(\hat{\mathbf{r}}) + \sqrt{l(l+1)} \frac{h_l^{(1)}(\kappa r)}{\kappa r} \mathbf{A}_{3,l,m}(\hat{\mathbf{r}}), \\ \tau &= 1, 2; \quad l = 1, 2, 3, \dots; \quad m = -l, -l+1, \dots, +l, \end{aligned}$$

¹Throughout this text, we use the letter κ for wave number in order to avoid confusion with Bloch vector \mathbf{k} and its magnitude, introduced in Section 3.

where $\mathbf{r} = r\hat{\mathbf{r}} = r(\sin\theta(\hat{\mathbf{x}}\cos\phi + \hat{\mathbf{y}}\sin\phi) + \hat{\mathbf{z}}\cos\theta)$; $j_l(x), h_l^{(1)}(x) = j_l(x) + iy_l(x)$ are the regular spherical Bessel function and spherical Hankel function of the first kind², respectively, as in [4, §10.47], and $\mathbf{A}_{\tau,l,m}$ are the *vector spherical harmonics*

$$\begin{aligned} \mathbf{A}_{1,l,m}(\hat{\mathbf{r}}) &= \frac{1}{\sqrt{l(l+1)}} \nabla \times (\mathbf{r}Y_{l,m}(\hat{\mathbf{r}})) = \frac{1}{\sqrt{l(l+1)}} \nabla Y_{l,m}(\hat{\mathbf{r}}) \times \mathbf{r}, \\ \mathbf{A}_{2,l,m}(\hat{\mathbf{r}}) &= \frac{1}{\sqrt{l(l+1)}} r \nabla Y_{l,m}(\hat{\mathbf{r}}), \\ (2.4) \quad \mathbf{A}_{3,l,m}(\hat{\mathbf{r}}) &= \hat{\mathbf{r}} Y_{l,m}(\hat{\mathbf{r}}). \end{aligned}$$

Note that the regular waves $\mathbf{v}_{\tau lm}$ (with fields expressed in cartesian coordinates) have all well-defined limits in the origin, and except for the “electric dipolar” waves \mathbf{v}_{21m} , they vanish. In our convention, the (scalar) spherical harmonics $Y_{l,m}$ are identical to those in [4, 14.30.1], i.e.

$$Y_{l,m}(\hat{\mathbf{r}}) = \left(\frac{(l-m)!(2l+1)}{4\pi(l+m)!} \right)^{\frac{1}{2}} e^{im\phi} P_l^m(\cos\theta)$$

where importantly, the Ferrers functions P_l^m defined as in [4, §14.3(i)] do already contain the Condon-Shortley phase $(-1)^m$. For later use, we also introduce “dual” spherical harmonics $Y'_{l,m}$ defined by duality relation with the “usual” spherical harmonics

$$(2.5) \quad \iint Y'_{l',m'}(\hat{\mathbf{r}}) Y_{l,m}(\hat{\mathbf{r}}) d\Omega = \delta_{\tau'\tau} \delta_{l'l} \delta_{m'm}$$

and corresponding dual vector spherical harmonics

$$(2.6) \quad \iint \mathbf{A}'_{\tau',l',m'}(\hat{\mathbf{r}}) \cdot \mathbf{A}_{\tau,l,m}(\hat{\mathbf{r}}) d\Omega = \delta_{\tau'\tau} \delta_{l'l} \delta_{m'm}$$

(complex conjugation not implied in the dot product here). In our convention, we have

$$\begin{aligned} Y_{l,m}(\hat{\mathbf{r}}) &= (Y_{l,m}(\hat{\mathbf{r}}))^* = (-1)^m Y_{l,-m}(\hat{\mathbf{r}}). \\ \mathbf{A}'_{\tau,l,m}(\hat{\mathbf{r}}) &= (\mathbf{A}_{\tau,l,m}(\hat{\mathbf{r}}))^* = (-1)^m \mathbf{A}_{\tau,l,-m}(\hat{\mathbf{r}}). \end{aligned}$$

The convention for VSWFs used here is the same as in [23]; over other conventions used elsewhere in literature, it has several fundamental advantages – most importantly, the translation operators introduced later in eq. (2.21) are unitary, and it gives the simplest possible expressions for power transport and cross sections without additional l, m -dependent factors (for that reason, we also call our VSWFs as *power-normalised*). Power-normalisation and unitary translation operators are possible to achieve also with real spherical harmonics – such a convention is used in [24].

²The interpretation of $\mathbf{u}_{\tau lm}(\kappa\mathbf{r})$ containing spherical Hankel functions of the first kind as *outgoing* waves at positive frequencies is associated with a specific choice of sign in the exponent of time-frequency transformation, $\psi(t) = (2\pi)^{-1/2} \int \psi(\omega) e^{-i\omega t} d\omega$. This matters especially when considering materials with gain or loss: in this convention, lossy materials will have refractive index (and wavenumber κ , at a given positive frequency) with *positive* imaginary part, and gain materials will have it negative and, for example, Drude-Lorentz model of a lossy medium will have poles in the lower complex half-plane.

2.1.2. *T-matrix definition.* The regular VSWFs $\mathbf{v}_{\tau lm}(\mathbf{r})$ would constitute a basis for solutions of the Helmholtz equation (2.1) inside a ball $B_{R>}(\mathbf{0})$ with radius $R>$ and center in the origin, were it filled with homogeneous isotropic medium; however, if the equation is not guaranteed to hold inside a smaller ball $\overline{B_{R<}(\mathbf{0})}$ around the origin (typically due to presence of a scatterer), one has to add the outgoing VSWFs $\mathbf{u}_{\tau lm}(\mathbf{r})$ to have a complete basis of the solutions in the volume $\Theta_{R<,R>}(\mathbf{0}) = B_{R>}(\mathbf{0}) \setminus \overline{B_{R<}(\mathbf{0})}$.

The single-particle scattering problem at frequency ω can be posed as follows: Let a scatterer be enclosed inside the ball $\overline{B_{R<}(\mathbf{0})}$ and let the whole volume $\Theta_{R<,R>}(\mathbf{0})$ be filled with a homogeneous isotropic medium with wave number $\kappa(\omega)$. Inside $\Theta_{R<,R>}(\mathbf{0})$, the electric field can be expanded as

$$(2.7) \quad \mathbf{E}(\omega, \mathbf{r}) = \sum_{\tau=1,2} \sum_{l=1}^{\infty} \sum_{m=-l}^{+l} (a_{\tau lm} \mathbf{v}_{\tau lm}(\kappa \mathbf{r}) + f_{\tau lm} \mathbf{u}_{\tau lm}(\kappa \mathbf{r})).$$

If there were no scatterer and $\overline{B_{R<}(\mathbf{0})}$ were filled with the same homogeneous medium, the part with the outgoing VSWFs would vanish and only the part $\mathbf{E}_{\text{inc}} = \sum_{\tau lm} a_{\tau lm} \mathbf{v}_{\tau lm}$ due to sources outside $B_{R>}(\mathbf{0})$ would remain. Let us assume that the “driving field” is given, so that presence of the scatterer does not affect \mathbf{E}_{inc} and is fully manifested in the latter part, $\mathbf{E}_{\text{scat}} = \sum_{\tau lm} f_{\tau lm} \mathbf{u}_{\tau lm}$. We also assume that the scatterer is made of optically linear materials and hence reacts to the incident field in a linear manner. This gives a linearity constraint between the expansion coefficients

$$(2.8) \quad f_{\tau lm} = \sum_{\tau' l' m'} T_{\tau lm; \tau' l' m'} a_{\tau' l' m'}$$

where the $T_{\tau lm; \tau' l' m'} = T_{\tau lm; \tau' l' m'}(\omega)$ are the elements of the *transition matrix*, a.k.a. *T-matrix*. It completely describes the scattering properties of a linear scatterer, so with the knowledge of the *T-matrix* we can solve the single-particle scattering problem simply by substituting appropriate expansion coefficients $a_{\tau' l' m'}$ of the driving field into (2.8). The outgoing VSWF expansion coefficients $f_{\tau lm}$ are the effective induced electric ($\tau = 2$) and magnetic ($\tau = 1$) multipole polarisation amplitudes of the scatterer, and this is why we sometimes refer to the corresponding VSWFs as to the electric and magnetic VSWFs, respectively.

T-matrices of particles with certain simple geometries (most famously spherical) can be obtained analytically [24, 33]; for particles with smooth surfaces one can find them numerically using the *null-field method* [54, 55, 24] which works well in the most typical cases, but for less common parameter ranges (such as concave shapes, extreme values of aspect ratios or relative refractive index) they might suffer from serious numerical instabilities [34, Sect. 5.8.4]. In general, elements of the *T-matrix* can be obtained by simulating scattering of a regular spherical wave $\mathbf{v}_{\tau lm}$ and projecting the scattered fields (or induced currents, depending on the method) onto the outgoing VSWFs $\mathbf{u}_{\tau' l' m'}$. In practice, one can compute only a finite number of elements with a cut-off value L on the multipole degree, $l, l' \leq L$, see below.

For the numerical evaluation of *T-matrices* for simple axially symmetric scatterers in QPMS, we typically use the null-field equations, and for more complicated

scatterers we use the `scuff-tmatrix` tool from the free software SCUFF-EM suite [43, 42].³

2.1.3. *T-matrix compactness, cutoff validity.* The magnitude of the T -matrix elements depends heavily on the scatterer's size compared to the wavelength. Typically,⁴ from certain multipole degree onwards, $l, l' > L$, the elements of the T -matrix are negligible, so truncating the T -matrix at finite multipole degree L gives a good approximation of the actual infinite-dimensional operator. If the incident field is well-behaved, i.e. the expansion coefficients $a_{\tau' l' m'}$ do not take excessive values for $l' > L$, the scattered field expansion coefficients $f_{\tau l m}$ with $l > L$ will also be negligible.

A rule of thumb to choose the L with desired T -matrix element accuracy δ can be obtained from the spherical Bessel function expansion around zero [4, 10.52.1] by requiring that $\delta \gg (nR)^L / (2L + 1)!!$, where R is the scatterer radius and n its (maximum) refractive index.

2.1.4. *Power transport.* For convenience, let us introduce a short-hand matrix notation for the expansion coefficients and related quantities, so that we do not need to write the indices explicitly; so for example, eq. (2.8) would be written as $f = Ta$, where a, f are column vectors with the expansion coefficients. Transposed and complex-conjugated matrices are labeled with the \dagger superscript.

With this notation, we state an important result about power transport, derivation of which can be found in [24, sect. 7.3]. Let the field in $\Theta_{R<,R>}(\mathbf{0})$ have expansion as in (2.7). Then the net power transported from $B_{R<}(\mathbf{0})$ to $\Theta_{R<,R>}(\mathbf{0})$ by electromagnetic radiation is

$$(2.9) \quad P = \frac{1}{2\kappa^2\eta_0\eta} \left(\Re(a^\dagger f) + \|f\|^2 \right) = \frac{1}{2\kappa^2\eta_0\eta} a^\dagger \left(T^\dagger T + \frac{T^\dagger + T}{2} \right) a,$$

where $\eta_0 = \sqrt{\mu_0/\varepsilon_0}$ and $\eta = \sqrt{\mu/\varepsilon}$ are wave impedance of vacuum and relative wave impedance of the medium in $\Theta_{R<,R>}(\mathbf{0})$, respectively. Here P is well-defined only when $\kappa^2\eta$ is real. In realistic scattering setups, power is transferred by radiation into $B_{R<}(\mathbf{0})$ and absorbed by the enclosed scatterer, so P is negative and its magnitude equals to power absorbed by the scatterer. In other words, the hermitian operator $\Pi = T^\dagger T + (T^\dagger + T)/2$ must be negative (semi-)definite for a particle without gain. This provides a simple but very useful sanity check on the numerically obtained T -matrices: non-negligible positive eigenvalues of Π indicate either too drastic multipole truncation or another problem with the T -matrix.

2.1.5. *Plane wave expansion.* In many scattering problems considered in practice, the driving field is at least approximately a plane wave. A transversal ($\hat{\mathbf{k}} \cdot \mathbf{E}_0 = 0$) plane wave propagating in direction $\hat{\mathbf{k}}$ with (complex) amplitude \mathbf{E}_0 can be

³Note that the upstream versions of SCUFF-EM contain a bug that renders almost all T -matrix results wrong; we found and fixed the bug in our fork available at <https://github.com/teknokrates/scuff-em> in revision g78689f5. However, the bugfix has not been merged into upstream by the time of writing this article.

⁴It has been proven that the T -matrix of a bounded scatterer is a compact operator for *acoustic* scattering problems [7]. While we conjecture that this holds also for bounded electromagnetic scatterers, we are not aware of a definitive proof.

expanded into regular VSWFs [24, 7.7.1] as

$$\mathbf{E}_{\text{PW}}(\mathbf{r}, \omega) = \mathbf{E}_0 e^{i\kappa \hat{\mathbf{k}} \cdot \mathbf{r}} = \sum_{\tau, l, m} a_{\tau lm} \left(\hat{\mathbf{k}}, \mathbf{E}_0 \right) \mathbf{v}_{\tau lm}(\kappa \mathbf{r}),$$

where the expansion coefficients are obtained from the scalar products of the amplitude and corresponding dual vector spherical harmonics

$$\begin{aligned} a_{1,1m} \left(\hat{\mathbf{k}}, \mathbf{E}_0 \right) &= 4\pi i^l \mathbf{A}'_{1,l,m} \left(\hat{\mathbf{k}} \right) \cdot \mathbf{E}_0, \\ (2.10) \quad a_{2,2m} \left(\hat{\mathbf{k}}, \mathbf{E}_0 \right) &= -4\pi i^{l+1} \mathbf{A}'_{2,l,m} \left(\hat{\mathbf{k}} \right) \cdot \mathbf{E}_0. \end{aligned}$$

2.1.6. Cross-sections (single-particle). With the T -matrix and expansion coefficients of plane waves in hand, we can state the expressions for cross-sections of a single scatterer. Assuming a non-lossy background medium, extinction, scattering and absorption cross sections of a single scatterer irradiated by a plane wave propagating in direction $\hat{\mathbf{k}}$ and (complex) amplitude \mathbf{E}_0 are [24, sect. 7.8.2]

$$(2.11) \quad \sigma_{\text{ext}}(\hat{\mathbf{k}}) = -\frac{1}{\kappa^2 \|\mathbf{E}_0\|^2} \Re(a^\dagger f) = -\frac{1}{2\kappa^2 \|\mathbf{E}_0\|^2} a^\dagger (T + T^\dagger) a,$$

$$(2.12) \quad \sigma_{\text{scat}}(\hat{\mathbf{k}}) = \frac{1}{\kappa^2 \|\mathbf{E}_0\|^2} \|f\|^2 = \frac{1}{\kappa^2 \|\mathbf{E}_0\|^2} a^\dagger (T^\dagger T) a,$$

$$\begin{aligned} \sigma_{\text{abs}}(\hat{\mathbf{k}}) &= \sigma_{\text{ext}}(\hat{\mathbf{k}}) - \sigma_{\text{scat}}(\hat{\mathbf{k}}) = -\frac{1}{\kappa^2 \|\mathbf{E}_0\|^2} \left(\Re(a^\dagger f) + \|f\|^2 \right) \\ (2.13) \quad &= -\frac{1}{\kappa^2 \|\mathbf{E}_0\|^2} a^\dagger \left(T^\dagger T + \frac{T^\dagger + T}{2} \right) a, \end{aligned}$$

where $a = a(\mathbf{k}, \mathbf{E}_0)$ is the vector of plane wave expansion coefficients as in (2.10).

2.2. Multiple scattering. If the system consists of multiple scatterers, the EM fields around each one can be expanded in analogous way. Let \mathcal{P} be an index set labeling the scatterers. We enclose each scatterer in a closed ball $\overline{B_{R_p}}(\mathbf{r}_p)$ such that the balls do not touch, $\overline{B_{R_p}}(\mathbf{r}_p) \cap \overline{B_{R_q}}(\mathbf{r}_q) = \emptyset; p, q \in \mathcal{P}$, so there is a non-empty spherical shell $\Theta_{R_p, R_p^>}(\mathbf{r}_p)$ around each one that contains only the background medium without any scatterers; we assume that all the relevant volume outside $\bigcap_{p \in \mathcal{P}} \overline{B_{R_p}}(\mathbf{r}_p)$ is filled with the same background medium. Then the EM field inside each $\Theta_{R_p, R_p^>}(\mathbf{r}_p)$ can be expanded in a way similar to (2.7), using VSWFs with origins shifted to the centre of the volume:

$$\begin{aligned} (2.14) \quad \mathbf{E}(\omega, \mathbf{r}) &= \sum_{\tau=1,2} \sum_{l=1}^{\infty} \sum_{m=-l}^{+l} (a_{p,\tau lm} \mathbf{v}_{\tau lm}(\kappa(\mathbf{r} - \mathbf{r}_p)) + f_{p,\tau lm} \mathbf{u}_{\tau lm}(\kappa(\mathbf{r} - \mathbf{r}_p))), \\ &\quad \mathbf{r} \in \Theta_{R_p, R_p^>}(\mathbf{r}_p). \end{aligned}$$

Unlike the single scatterer case, the incident field coefficients $a_{p,\tau lm}$ here are not only due to some external driving field that the particle does not influence but they also contain the contributions of fields scattered from *all other scatterers*:

$$(2.15) \quad a_p = \tilde{a}_p + \sum_{q \in \mathcal{P} \setminus \{p\}} \mathcal{S}_{p \leftarrow q} f_q$$

where \tilde{a}_p represents the part due to the external driving that the scatterers can not influence, and $\mathcal{S}_{p \leftarrow q}$ is a *translation operator* defined below in Sec. 2.2.1, that contains the re-expansion coefficients of the outgoing waves in origin \mathbf{r}_q into regular waves in origin \mathbf{r}_p . For each scatterer, we also have its T -matrix relation as in (2.8),

$$f_q = T_q a_q.$$

Together with (2.15), this gives rise to a set of linear equations

$$(2.16) \quad f_p - T_p \sum_{q \in \mathcal{P} \setminus \{p\}} \mathcal{S}_{p \leftarrow q} f_q = T_p \tilde{a}_p, \quad p \in \mathcal{P}$$

which defines the multiple-scattering problem. If all the p, q -indexed vectors and matrices (note that without truncation, they are infinite-dimensional) are arranged into blocks of even larger vectors and matrices, this can be written in a short-hand form

$$(2.17) \quad (I - TS)f = T\tilde{a}$$

where I is the identity matrix, T is a block-diagonal matrix containing all the individual T -matrices, and \mathcal{S} contains the individual $\mathcal{S}_{p \leftarrow q}$ matrices as the off-diagonal blocks, whereas the diagonal blocks are set to zeros.

We note that eq. (2.17) with zero right-hand side describes the normal modes of the system; the methods mentioned later in Section (3) for solving the band structure of a periodic system can be used as well for finding the resonant frequencies of a finite system.

In practice, the multiple-scattering problem is solved in its truncated form, in which all the l -indices related to a given scatterer p are truncated as $l \leq L_p$, leaving only $N_p = 2L_p(L_p + 2)$ different τlm -multi-indices left. The truncation degree can vary for different scatterers (e.g. due to different physical sizes), so the truncated block $[\mathcal{S}_{p \leftarrow q}]_{l_q \leq L_q, l_p \leq L_p}$ has shape $N_p \times N_q$, not necessarily square.

If no other type of truncation is done, there remain $2L_p(L_p + 2)$ different τlm -multi-indices for the p -th scatterer, so that the truncated version of the matrix $(I - TS)$ is a square matrix with $\left(\sum_{p \in \mathcal{P}} N_p\right)^2$ elements in total. The truncated problem (2.17) can then be solved using standard numerical linear algebra methods (typically, by LU factorisation of the $(I - TS)$ matrix at a given frequency, and then solving with Gauss elimination for as many different incident \tilde{a} vectors as needed).

Alternatively, the multiple scattering problem can be formulated in terms of the regular field expansion coefficients,

$$a_p - \sum_{q \in \mathcal{P} \setminus \{p\}} \mathcal{S}_{p \leftarrow q} T_q a_q = \tilde{a}_p, \quad p \in \mathcal{P},$$

$$(I - ST)a = \tilde{a},$$

but this form is less suitable for numerical calculations due to the fact that the regular VSWF expansion coefficients on both sides of the equation are typically non-negligible even for large multipole degree l , hence the truncation is not justified in this case.

2.2.1. *Translation operator.* Let $\mathbf{r}_1, \mathbf{r}_2$ be two different origins; a regular VSWF with origin \mathbf{r}_1 can be expanded in terms of regular VSWFs with origin \mathbf{r}_2 as follows:

$$(2.18) \quad \mathbf{v}_{\tau lm}(\kappa(\mathbf{r} - \mathbf{r}_1)) = \sum_{\tau' l' m'} \mathcal{R}_{\tau lm; \tau' l' m'}(\kappa(\mathbf{r}_2 - \mathbf{r}_1)) \mathbf{v}_{\tau' l' m'}(\mathbf{r} - \mathbf{r}_2),$$

where an explicit formula for the regular translation operator \mathcal{R} reads in eq. (2.24) below. For singular (outgoing) waves, the form of the expansion differs inside and outside the ball $B_{\|\mathbf{r}_2 - \mathbf{r}_1\|}(\mathbf{r}_1)$:

$$(2.19) \quad \mathbf{u}_{\tau lm}(\kappa(\mathbf{r} - \mathbf{r}_1)) = \begin{cases} \sum_{\tau' l' m'} \mathcal{S}_{\tau lm; \tau' l' m'}(\kappa(\mathbf{r}_2 - \mathbf{r}_1)) \mathbf{v}_{\tau' l' m'}(\kappa(\mathbf{r} - \mathbf{r}_2)), & \mathbf{r} \in B_{\|\mathbf{r}_1 - \mathbf{r}_2\|}(\mathbf{r}_2) \\ \sum_{\tau' l' m'} \mathcal{R}_{\tau lm; \tau' l' m'}(\kappa(\mathbf{r}_2 - \mathbf{r}_1)) \mathbf{u}_{\tau' l' m'}(\kappa(\mathbf{r} - \mathbf{r}_2)), & \mathbf{r} \notin B_{\|\mathbf{r}_1 - \mathbf{r}_2\|}(\mathbf{r}_2) \end{cases},$$

where the singular translation operator \mathcal{S} has the same form as \mathcal{R} in (2.24) except the regular spherical Bessel functions j_l are replaced with spherical Hankel functions $h_l^{(1)}$.

As MSTMM deals most of the time with the *expansion coefficients* of fields $a_{p, \tau lm}, f_{p, \tau lm}$ in different origins \mathbf{r}_p rather than with the VSWFs directly, let us write down how *they* transform under translation. We assume the field can be expressed in terms of regular waves everywhere, and expand it in two different origins $\mathbf{r}_p, \mathbf{r}_q$,

$$\mathbf{E}(\mathbf{r}, \omega) = \sum_{\tau, l, m} a_{p, \tau lm} \mathbf{v}_{\tau lm}(\kappa(\mathbf{r} - \mathbf{r}_p)) = \sum_{\tau', l', m'} a_{q, \tau' l' m'} \mathbf{v}_{\tau' l' m'}(\kappa(\mathbf{r} - \mathbf{r}_q)).$$

Re-expanding the waves around \mathbf{r}_p in terms of waves around \mathbf{r}_q using (2.18),

$$\mathbf{E}(\mathbf{r}, \omega) = \sum_{\tau, l, m} a_{p, \tau lm} \sum_{\tau' l' m'} \mathcal{R}_{\tau lm; \tau' l' m'}(\kappa(\mathbf{r}_q - \mathbf{r}_p)) \mathbf{v}_{\tau' l' m'}(\kappa(\mathbf{r} - \mathbf{r}_q))$$

and comparing to the original expansion around \mathbf{r}_q , we obtain

$$(2.20) \quad a_{q, \tau' l' m'} = \sum_{\tau, l, m} \mathcal{R}_{\tau lm; \tau' l' m'}(\kappa(\mathbf{r}_q - \mathbf{r}_p)) a_{p, \tau lm}.$$

For the sake of readability, we introduce a shorthand matrix form for (2.20)

$$(2.21) \quad a_q = \mathcal{R}_{q \leftarrow p} a_p$$

(note the reversed indices) Similarly, if we had only outgoing waves in the original expansion around \mathbf{r}_p , we would get

$$(2.22) \quad a_q = \mathcal{S}_{q \leftarrow p} f_p$$

for the expansion inside the ball $B_{\|\mathbf{r}_q - \mathbf{r}_p\|}(\mathbf{r}_p)$ and

$$(2.23) \quad f_q = \mathcal{R}_{q \leftarrow p} f_p$$

outside.

In our convention, the regular translation operator elements can be expressed explicitly as

$$(2.24) \quad \mathcal{R}_{\tau lm; \tau' l' m'}(\mathbf{d}) = \sum_{\lambda=|l-l'|+|\tau-\tau'|}^{l+l'} C_{\tau lm; \tau' l' m'}^{\lambda} Y_{\lambda, m-m'}(\hat{\mathbf{d}}) j_{\lambda}(d),$$

and analogously the elements of the singular operator \mathcal{S} , having spherical Hankel functions ($h_l^{(1)} = j_l + iy_l$) in the radial part instead of the regular Bessel functions,

$$(2.25) \quad \mathcal{S}_{\tau lm; \tau' l' m'}(\mathbf{d}) = \sum_{\lambda=|l-l'|+|\tau-\tau'|}^{l+l'} C_{\tau lm; \tau' l' m'}^{\lambda} Y_{\lambda, m-m'}(\hat{\mathbf{d}}) h_{\lambda}^{(1)}(d),$$

where the constant factors in our convention read

$$(2.26) \quad \begin{aligned} C_{\tau lm; \tau' l' m'}^{\lambda} &= \begin{cases} A_{lm; l' m'}^{\lambda} & \tau = \tau', \\ B_{lm; l' m'}^{\lambda} & \tau \neq \tau', \end{cases} \\ A_{lm; l' m'}^{\lambda} &= (-1)^{\frac{l'-l+\lambda}{2}} \sqrt{\frac{4\pi(2\lambda+1)(2l+1)(2l'+1)}{l(l+1)l'(l'+1)}} \times \\ &\quad \times \begin{pmatrix} l & l' & \lambda \\ 0 & 0 & 0 \end{pmatrix} \begin{pmatrix} l & l' & \lambda \\ m & -m' & m'-m \end{pmatrix} (l(l+1) + l'(l'+1) - \lambda(\lambda+1)), \\ B_{lm; l' m'}^{\lambda} &= -i(-1)^{\frac{l'-l+\lambda+1}{2}} \sqrt{\frac{4\pi(2\lambda+1)(2l+1)(2l'+1)}{l(l+1)l'(l'+1)}} \times \\ &\quad \times \begin{pmatrix} l & l' & \lambda-1 \\ 0 & 0 & 0 \end{pmatrix} \begin{pmatrix} l & l' & \lambda \\ m & -m' & m'-m \end{pmatrix} \sqrt{\lambda^2 - (l-l')^2} \sqrt{(l+l'+1)^2 - \lambda^2}. \end{aligned}$$

Here $\begin{pmatrix} l_1 & l_2 & l_3 \\ m_1 & m_2 & m_3 \end{pmatrix}$ is the $3j$ symbol defined as in [4, §34.2]. Importantly for practical calculations, these rather complicated coefficients need to be evaluated only once up to the highest truncation order, $l, l' \leq L$.

In our convention, the regular translation operator is unitary, $(\mathcal{R}_{\tau lm; \tau' l' m'}(\mathbf{d}))^{-1} = \mathcal{R}_{\tau lm; \tau' l' m'}(-\mathbf{d}) = \mathcal{R}_{\tau' l' m'; \tau lm}^*(\mathbf{d})$, or in the per-particle matrix notation,

$$(2.27) \quad \mathcal{R}_{q \leftarrow p}^{-1} = \mathcal{R}_{p \leftarrow q} = \mathcal{R}_{q \leftarrow p}^{\dagger}.$$

Note that truncation at finite multipole degree breaks the unitarity, $[\mathcal{R}_{q \leftarrow p}]_{l \leq L}^{-1} \neq [\mathcal{R}_{p \leftarrow q}]_{l \leq L} = [\mathcal{R}_{q \leftarrow p}^{\dagger}]_{l \leq L}$, which has to be taken into consideration when evaluating quantities such as absorption or scattering cross sections. Similarly, the full regular operators can be composed

$$(2.28) \quad \mathcal{R}_{a \leftarrow c} = \mathcal{R}_{a \leftarrow b} \mathcal{R}_{b \leftarrow c}$$

but truncation breaks this, $[\mathcal{R}_{a \leftarrow c}]_{l \leq L} \neq [\mathcal{R}_{a \leftarrow b}]_{l \leq L} [\mathcal{R}_{b \leftarrow c}]_{l \leq L}$.

2.2.2. Cross-sections (many scatterers). For a system of many scatterers, Kristensson [24, sect. 9.2.2] derives only the extinction cross section formula. Let us re-derive it together with the many-particle scattering and absorption cross sections. First, let us take a ball containing all the scatterers at once, $B_R(\mathbf{r}_{\square}) \supset \bigcup_{p \in \mathcal{P}} \overline{B_{R_p}(\mathbf{r}_p)}$. Outside $B_R(\mathbf{r}_{\square})$, we can describe the EM fields as if there was only a single scatterer,

$$\mathbf{E}(\mathbf{r}) = \sum_{\tau, l, m} (a_{\square, \tau lm} \mathbf{v}_{\tau lm}(\kappa(\mathbf{r} - \mathbf{r}_{\square})) + f_{\square, \tau lm} \mathbf{u}_{\tau lm}(\kappa(\mathbf{r} - \mathbf{r}_{\square}))),$$

where a_{\square}, f_{\square} are the vectors of VSWF expansion coefficients of the incident and total scattered fields, respectively, at origin \mathbf{r}_{\square} . In principle, one could evaluate f_{\square} using the translation operators and use the single-scatterer formulae (2.11)–(2.13)

with $a = a_\square, f = f_\square$ to obtain the cross sections. However, this is not suitable for numerical evaluation with truncation in multipole degree; hence we need to express them in terms of particle-wise expansions a_p, f_p . The original incident field re-expanded around p -th particle reads according to (2.21)

$$(2.29) \quad \tilde{a}_p = \mathcal{R}_{p \leftarrow \square} a_\square$$

whereas the contributions of fields scattered from each particle expanded around the global origin \mathbf{r}_\square is, according to (2.22),

$$(2.30) \quad f_\square = \sum_{q \in \mathcal{P}} \mathcal{R}_{\square \leftarrow q} f_q.$$

Using the unitarity (2.27) and composition (2.28) properties, one has

$$(2.31) \quad \begin{aligned} a_\square^\dagger f_\square &= \tilde{a}_p^\dagger \mathcal{R}_{p \leftarrow \square} \mathcal{R}_{\square \leftarrow q} f_q = \tilde{a}_p^\dagger \sum_{q \in \mathcal{P}} \mathcal{R}_{p \leftarrow q} f_q \\ &= \sum_{q \in \mathcal{P}} (\mathcal{R}_{q \leftarrow p} \tilde{a}_p)^\dagger f_q = \sum_{q \in \mathcal{P}} \tilde{a}_q^\dagger f_q, \end{aligned}$$

where only the last expression is suitable for numerical evaluation with truncated matrices, because the previous ones contain a translation operator right next to an incident field coefficient vector. Similarly,

$$(2.32) \quad \begin{aligned} \|f_\square\|^2 &= f_\square^\dagger f_\square = \sum_{p \in \mathcal{P}} (\mathcal{R}_{\square \leftarrow p} f_p)^\dagger \sum_{q \in \mathcal{P}} \mathcal{R}_{\square \leftarrow q} f_q \\ &= \sum_{p \in \mathcal{P}} \sum_{q \in \mathcal{P}} f_p^\dagger \mathcal{R}_{p \leftarrow q} f_q. \end{aligned}$$

Substituting (2.31), (2.32) into (2.12) and (2.13), we get the many-particle expressions for extinction, scattering and absorption cross sections suitable for numerical evaluation:

$$(2.33)_{\text{xt}} \quad \begin{aligned} \left(\hat{\mathbf{k}}, \hat{\mathbf{E}}_0 \right) &= -\frac{1}{\kappa^2 \|\mathbf{E}_0\|^2} \Re \sum_{p \in \mathcal{P}} \tilde{a}_p^\dagger f_p = -\frac{1}{2k^2 \|\mathbf{E}_0\|^2} \Re \sum_{p \in \mathcal{P}} \tilde{a}_p^\dagger (T_p + T_p^\dagger) a_p, \\ \sigma_{\text{scat}} \left(\hat{\mathbf{k}}, \hat{\mathbf{E}}_0 \right) &= \frac{1}{\kappa^2 \|\mathbf{E}_0\|^2} \sum_{p \in \mathcal{P}} \sum_{q \in \mathcal{P}} f_p^\dagger \mathcal{R}_{p \leftarrow q} f_q \\ (2.34) \quad &= \frac{1}{\kappa^2 \|\mathbf{E}_0\|^2} \sum_{p \in \mathcal{P}} \sum_{q \in \mathcal{P}} a_p^\dagger T_p^\dagger \mathcal{R}_{p \leftarrow q} T_q a_q, \\ \sigma_{\text{abs}} \left(\hat{\mathbf{k}}, \hat{\mathbf{E}}_0 \right) &= -\frac{1}{\kappa^2 \|\mathbf{E}_0\|^2} \sum_{p \in \mathcal{P}} \Re \left(f_p^\dagger \left(\tilde{a}_p + \sum_{q \in \mathcal{P}} \mathcal{R}_{p \leftarrow q} f_q \right) \right). \end{aligned}$$

(2.35)

An alternative approach to derive the absorption cross section is via a power transport argument. Note the direct proportionality between absorption cross section (2.13) and net radiated power for single scatterer (2.9), $\sigma_{\text{abs}} = -\eta_0 \eta P / 2 \|\mathbf{E}_0\|^2$. In the many-particle setup (with non-lossy background medium, so that only the particles absorb), the total absorbed power is equal to the sum of absorbed powers on each particle, $-P = \sum_{p \in \mathcal{P}} -P_p$. Using the power transport formula (2.9)

particle-wise gives

$$(2.36) \quad \sigma_{\text{abs}}(\hat{\mathbf{k}}) = -\frac{1}{\kappa^2 \|\mathbf{E}_0\|^2} \sum_{p \in \mathcal{P}} \left(\Re(a_p^\dagger f_p) + \|f_p\|^2 \right)$$

which seems different from (2.35), but using (2.15), we can rewrite it as

$$\begin{aligned} \sigma_{\text{abs}}(\hat{\mathbf{k}}) &= -\frac{1}{\kappa^2 \|\mathbf{E}_0\|^2} \sum_{p \in \mathcal{P}} \Re(f_p^\dagger (a_p + f_p)) \\ &= -\frac{1}{\kappa^2 \|\mathbf{E}_0\|^2} \sum_{p \in \mathcal{P}} \Re \left(f_p^\dagger \left(\tilde{a}_p + \sum_{q \in \mathcal{P} \setminus \{p\}} \mathcal{S}_{p \leftarrow q} f_q + f_p \right) \right). \end{aligned}$$

It is easy to show that all the terms of $\sum_{p \in \mathcal{P}} \sum_{q \in \mathcal{P} \setminus \{p\}} f_p^\dagger \mathcal{S}_{p \leftarrow q} f_q$ containing the sin-

gular spherical Bessel functions y_l are imaginary, so that actually $\sum_{p \in \mathcal{P}} \Re \left(\sum_{q \in \mathcal{P} \setminus \{p\}} f_p^\dagger \mathcal{S}_{p \leftarrow q} f_q + f_p^\dagger f_p \right) = \sum_{p \in \mathcal{P}} \Re \left(\sum_{q \in \mathcal{P} \setminus \{p\}} f_p^\dagger \mathcal{R}_{p \leftarrow q} f_q + f_p^\dagger f_p \right) = \sum_{p \in \mathcal{P}} \sum_{q \in \mathcal{P}} f_p^\dagger \mathcal{R}_{p \leftarrow q} f_q$, proving that the expressions in (2.35) and (2.36) are equal.

3. INFINITE PERIODIC SYSTEMS

Although large finite systems are where MSTMM excels the most, there are several reasons that makes its extension to infinite lattices (where periodic boundary conditions might be applied) desirable as well. Other methods might be already fast enough, but MSTMM will be faster in most cases in which there is enough spacing between the neighboring particles. MSTMM works well with any space group symmetry the system might have (as opposed to, for example, FDTD with a cubic mesh applied to a honeycomb lattice), which makes e.g. application of group theory in mode analysis quite easy. And finally, having a method that handles well both infinite and large finite systems gives a possibility to study finite-size effects in periodic scatterer arrays.

3.1. Formulation of the problem. Let us have a linear system of compact EM scatterers on a homogeneous background as in Section (2.2), but this time, the system shall be periodic: let there be a d -dimensional (d can be 1, 2 or 3) Bravais lattice embedded into the three-dimensional real space, with lattice vectors $\{\mathbf{a}_i\}_{i=1}^d$, and let the lattice points be labeled with an d -dimensional integer multi-index $\mathbf{n} \in \mathbb{Z}^d$, so the lattice points have cartesian coordinates $\mathbf{R}_{\mathbf{n}} = \sum_{i=1}^d n_i \mathbf{a}_i$. There can be several scatterers per unit cell with indices α from a set \mathcal{P}_1 and (relative) positions \mathbf{r}_{α} inside the unit cell; any particle of the periodic system can thus be labeled by a multi-index from $\mathcal{P} = \mathbb{Z}^d \times \mathcal{P}_1$. The scatterers are located at positions $\mathbf{r}_{\mathbf{n},\alpha} = \mathbf{R}_{\mathbf{n}} + \mathbf{r}_{\alpha}$ and their T -matrices are periodic, $T_{\mathbf{n},\alpha} = T_{\alpha}$. In such system, the multiple-scattering problem (2.16) can be rewritten as

$$(3.1) \quad f_{\mathbf{n},\alpha} - T_{\alpha} \sum_{(\mathbf{m},\beta) \in \mathcal{P} \setminus \{(\mathbf{n},\alpha)\}} \mathcal{S}_{\mathbf{n},\alpha \leftarrow \mathbf{m},\beta} f_{\mathbf{m},\beta} = T_{\alpha} \tilde{a}_{\mathbf{n},\alpha}. \quad (\mathbf{n},\alpha) \in \mathcal{P}$$

Due to periodicity, we can also write $\mathcal{S}_{\mathbf{n},\alpha \leftarrow \mathbf{m},\beta} = \mathcal{S}_{\alpha \leftarrow \beta}(\mathbf{R}_{\mathbf{m}} - \mathbf{R}_{\mathbf{n}}) = \mathcal{S}_{\alpha \leftarrow \beta}(\mathbf{R}_{\mathbf{m}-\mathbf{n}}) = \mathcal{S}_{\mathbf{0},\alpha \leftarrow \mathbf{m}-\mathbf{n},\beta}$. Assuming quasi-periodic right-hand side with quasi-momentum \mathbf{k} , $\tilde{a}_{\mathbf{n},\alpha} = \tilde{a}_{\mathbf{0},\alpha}(\mathbf{k}) e^{i\mathbf{k} \cdot \mathbf{R}_{\mathbf{n}}}$, the solutions of (3.1) will be also quasi-periodic according to Bloch theorem, $f_{\mathbf{n},\alpha} = f_{\mathbf{0},\alpha}(\mathbf{k}) e^{i\mathbf{k} \cdot \mathbf{R}_{\mathbf{n}}}$, and eq. (3.1) can be rewritten as follows

$$\begin{aligned} f_{\mathbf{0},\alpha}(\mathbf{k}) e^{i\mathbf{k} \cdot \mathbf{R}_{\mathbf{n}}} - T_{\alpha} \sum_{(\mathbf{m},\beta) \in \mathcal{P} \setminus \{(\mathbf{n},\alpha)\}} \mathcal{S}_{\mathbf{n},\alpha \leftarrow \mathbf{m},\beta} f_{\mathbf{0},\beta}(\mathbf{k}) e^{i\mathbf{k} \cdot \mathbf{R}_{\mathbf{m}}} &= T_{\alpha} \tilde{a}_{\mathbf{0},\alpha}(\mathbf{k}) e^{i\mathbf{k} \cdot \mathbf{R}_{\mathbf{n}}}, \\ f_{\mathbf{0},\alpha}(\mathbf{k}) - T_{\alpha} \sum_{(\mathbf{m},\beta) \in \mathcal{P} \setminus \{(\mathbf{n},\alpha)\}} \mathcal{S}_{\mathbf{0},\alpha \leftarrow \mathbf{m}-\mathbf{n},\beta} f_{\mathbf{0},\beta}(\mathbf{k}) e^{i\mathbf{k} \cdot \mathbf{R}_{\mathbf{m}-\mathbf{n}}} &= T_{\alpha} \tilde{a}_{\mathbf{0},\alpha}(\mathbf{k}), \\ f_{\mathbf{0},\alpha}(\mathbf{k}) - T_{\alpha} \sum_{(\mathbf{m},\beta) \in \mathcal{P} \setminus \{(\mathbf{0},\alpha)\}} \mathcal{S}_{\mathbf{0},\alpha \leftarrow \mathbf{m},\beta} f_{\mathbf{0},\beta}(\mathbf{k}) e^{i\mathbf{k} \cdot \mathbf{R}_{\mathbf{m}}} &= T_{\alpha} \tilde{a}_{\mathbf{0},\alpha}(\mathbf{k}), \\ (3.2) \quad f_{\mathbf{0},\alpha}(\mathbf{k}) - T_{\alpha} \sum_{\beta \in \mathcal{P}} W_{\alpha\beta}(\mathbf{k}) f_{\mathbf{0},\beta}(\mathbf{k}) &= T_{\alpha} \tilde{a}_{\mathbf{0},\alpha}(\mathbf{k}), \end{aligned}$$

so we reduced the initial scattering problem to one involving only the field expansion coefficients from a single unit cell, but we need to compute the “lattice Fourier transform” of the translation operator,

$$(3.3) \quad W_{\alpha\beta}(\mathbf{k}) \equiv \sum_{\mathbf{m} \in \mathbb{Z}^d} (1 - \delta_{\alpha\beta} \delta_{\mathbf{m}\mathbf{0}}) \mathcal{S}_{\mathbf{0},\alpha \leftarrow \mathbf{m},\beta} e^{i\mathbf{k} \cdot \mathbf{R}_{\mathbf{m}}},$$

evaluation of which is possible but rather non-trivial due to the infinite lattice sum, so we cover it separately in Sect. (3.3).

As in the case of a finite system, eq. (3.2) can be written in a shorter block-matrix form,

$$(3.4) \quad (I - TW) f_0(\mathbf{k}) = T\tilde{a}_0(\mathbf{k})$$

Eq. (3.2) can be used to calculate electromagnetic response of the structure to external quasiperiodic driving field – most notably a plane wave. However, the non-trivial solutions of the equation with right hand side (i.e. the external driving) set to zero,

$$(3.5) \quad (I - TW) f_0(\mathbf{k}) = 0,$$

describes the *lattice modes*, i.e. electromagnetic excitations that can sustain themselves for prolonged time even without external driving. Non-trivial solutions to (3.5) exist if the matrix on the left-hand side $M(\omega, \mathbf{k}) = (I - T(\omega)W(\omega, \mathbf{k}))$ is singular – this condition gives the *dispersion relation* for the periodic structure. Note that in realistic (lossy) systems, at least one of the pair ω, \mathbf{k} will acquire complex values. The solution $f_0(\mathbf{k})$ is then obtained as the right singular vector of $M(\omega, \mathbf{k})$ corresponding to the zero singular value.

Loss in the scatterers causes the solutions of (3.5) shift to complex frequencies. If the background medium has constant real refractive index n , negative (or positive) imaginary part of the frequency ω causes an artificial gain (or loss) in the medium, which manifests itself as exponential magnification (or attenuation) of the radial parts of the translation operators, $h_l^{(1)}(rn\omega/c)$, w.r.t. the distance; the gain might then balance the losses in particles, resulting in sustained modes satisfying eq. (3.5).

3.2. Numerical solution. In practice, equation (3.4) is solved in the same way as eq. (2.17) in the multipole degree truncated form. The lattice mode problem (3.5) is (after multipole degree truncation) solved by finding ω, \mathbf{k} for which the matrix $M(\omega, \mathbf{k})$ has a zero singular value. A naïve approach to do that is to sample a volume with a grid in the (ω, \mathbf{k}) space, performing a singular value decomposition of $M(\omega, \mathbf{k})$ at each point and finding where the lowest singular value of $M(\omega, \mathbf{k})$ is close enough to zero. However, this approach is quite expensive, since $W(\omega, \mathbf{k})$ has to be evaluated for each ω, \mathbf{k} pair separately (unlike the original finite case (2.17) translation operator \mathcal{S} , which, for a given geometry, depends only on frequency). Therefore, a much more efficient but not completely robust approach to determine the photonic bands is to sample the \mathbf{k} -space (a whole Brillouin zone or its part) and for each fixed \mathbf{k} to find a corresponding frequency ω with zero singular value of $M(\omega, \mathbf{k})$ using a minimisation algorithm (two- or one-dimensional, depending on whether one needs the exact complex-valued ω or whether the its real-valued approximation is satisfactory). Typically, a good initial guess for $\omega(\mathbf{k})$ is obtained from the empty lattice approximation, $|\mathbf{k}| = \sqrt{\epsilon\mu}\omega/c_0$ (modulo reciprocal lattice points). A somehow challenging step is to distinguish the different bands that can all be very close to the empty lattice approximation, especially if the particles in the system are small. In high-symmetry points of the Brillouin zone, this can be solved by factorising $M(\omega, \mathbf{k})$ into irreducible representations Γ_i and performing the minimisation in each irrep separately, cf. Section 4, and using the different $\omega_{\Gamma_i}(\mathbf{k})$ to obtain the initial guesses for the nearby points $\mathbf{k} + \delta\mathbf{k}$.

An alternative, faster and more robust approach to generic minimisation algorithms are eigensolvers for nonlinear eigenvalue problems based on contour integration [1, 9] which are able to find the roots of $M(\omega, \mathbf{k}) = 0$ inside an area enclosed by

a given complex frequency plane contour, assuming that $M(\omega, \mathbf{k})$ is an analytical function of ω inside the contour. A necessary prerequisite for this is that all the ingredients of $M(\omega, \mathbf{k})$ are analytical as well. In practice, this usually means that interpolation cannot be used in a straightforward way for material properties or T -matrices. For material response, constant permittivity or Drude-Lorentz models suit this purpose well. The need to evaluate the T -matrices precisely (without the speedup provided by interpolation) at many points might cause a performance bottleneck for scatterers with more complicated shapes. And finally, the integration contour has to evade any branch cuts appearing in the lattice-summed translation operator $W(\omega, \mathbf{k})$, as described in the following and illustrated in Fig. 3.1.

3.3. Computing the lattice sum of the translation operator. The problem in evaluating (3.3) is the asymptotic behaviour of the translation operator at large distances, $\mathcal{S}_{0,\alpha \leftarrow \mathbf{m},\beta} \sim |\mathbf{R}_{\mathbf{m}}|^{-1} e^{i\kappa|\mathbf{R}_{\mathbf{m}}|}$, so that its lattice sum does not in the strict sense converge for any $d > 1$ -dimensional lattice unless $\Im\kappa > 0$. The problem of poorly converging lattice sums can be solved by decomposing the lattice-summed function into two parts: a short-range part that decays fast and can be summed directly, and a long-range part which decays poorly but is fairly smooth everywhere, so that its Fourier transform decays fast enough, and to deal with the long range part by Poisson summation over the reciprocal lattice; these two parts put together shall give an analytical continuation of the original sum for $\Im\kappa \leq 0$. This idea dates back to Ewald [6] who solved the problem for electrostatic potentials (Green's functions for Laplace's equation). For linear electrodynamic problems, ruled by Helmholtz equation, the same basic idea can be used as well, resulting in exponentially convergent summation formulae, but the technical details are considerably more complicated than in electrostatics. For the scalar Helmholtz equation in three dimensions, the formulae for lattice Green's functions were developed by Ham & Segall [13] for 3D periodicity, Kambe [17, 18, 19] for 2D periodicity and Moroz [35] for 1D periodicity. A review of these methods can be found in [26].

For our purposes we do not need directly the lattice Green's functions but rather the related lattice sums of spherical wavefunctions defined in (3.7), which can be derived by an analogous procedure. Below, we state the results in a form independent upon the normalisation and phase conventions for spherical harmonic bases (pointing out some errors in the aforementioned literature) and discuss some practical aspects of the numerical evaluation. The derivation of the somewhat more complicated 1D and 2D periodicities is provided in the Supplementary Material.

We note that the lattice sums for *scalar* Helmholtz equation are enough for the evaluation of the translation operator lattice sum $W_{\alpha\beta}(\mathbf{k})$: in eq. (2.25) we demonstratively expressed the translation operator elements as linear combinations of (outgoing) *scalar* spherical wavefunctions

$$(3.6) \quad \psi_{l,m}(\mathbf{r}) = h_l^{(1)}(r) Y_{l,m}(\hat{\mathbf{r}}).$$

If we formally label

$$(3.7) \quad \sigma_{l,m}(\mathbf{k}, \mathbf{s}) = \sum_{\mathbf{n} \in \mathbb{Z}^d} (1 - \delta_{\mathbf{R}_{\mathbf{n}}, \mathbf{s}}) e^{i\mathbf{k} \cdot \mathbf{R}_{\mathbf{n}}} \psi_{l,m}(\kappa(\mathbf{s} + \mathbf{R}_{\mathbf{n}})),$$

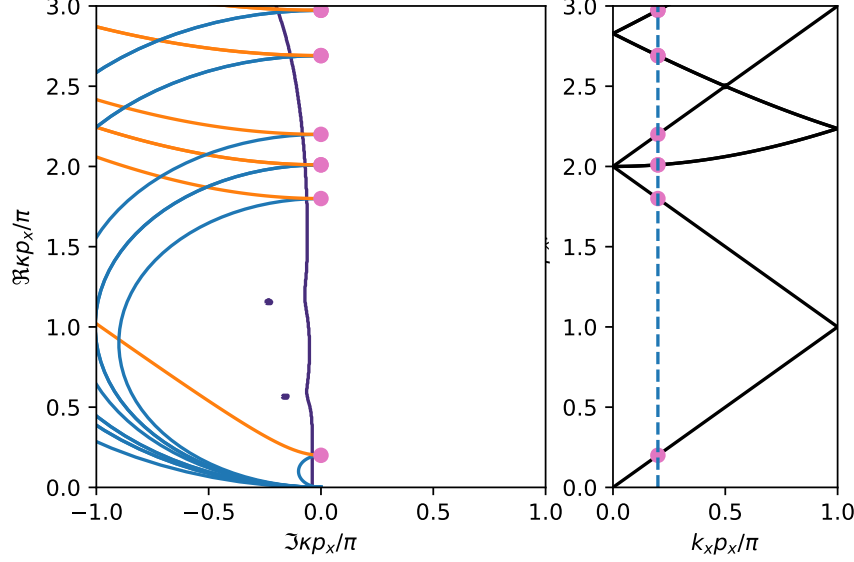


FIGURE 3.1. Left: Illustration of branch cuts in $M(\omega, \mathbf{k})$ obtained using Ewald summation over two-dimensional square lattice in three-dimensional space filled with dielectric medium with constant real refractive index n and wavenumber $\kappa(\omega) = \omega n/c$. The function is holomorphic in the positive imaginary half-plane. The points corresponding to the diffraction orders of an “empty” lattice lie on the real axis (pink), and from each of them two branch cuts originate: one due to the branch cut in the incomplete Γ function (orange, hyperbolic shape), and another due to the branch cut of $\gamma(z)$ if the branch is selected to be continuous for $-3\pi/2 < \arg(z-1) < \pi/2$ (blue, circular shape). Further non-analyticities might stem from the material model: the violet curve represents a branch cut originating from a complex square root in the refractive index $n_{\text{Au}}(\omega) = \sqrt{\varepsilon_{\text{Au}}(\omega)}$, where $\varepsilon_{\text{Au}}(\omega)$ is the Drude-Lorentz permittivity model of gold used for the scatterers. The other parameters used here are $p_x = 580 \text{ nm}$ (lattice period), $\mathbf{k} = (0.2\pi/p_x, 0)$, $n = 1.52$. The plot on the right shows the “empty” lattice diffraction orders on the line $\mathbf{k} = (k_x, 0)$, $k_x \in [0, \pi/p_x]$.

we see from eqs. (2.25),(3.3) that the matrix elements of $W_{\alpha\beta}(\mathbf{k})$ read

$$W_{\alpha,\tau lm;\beta,\tau' l' m'}(\mathbf{k}) = \sum_{\lambda=|l-l'|+|\tau-\tau'|}^{l+l'} C_{\tau lm;\tau' l' m'}^{\lambda} \sigma_{\lambda, m-m'}(-\mathbf{k}, \mathbf{r}_{\alpha} - \mathbf{r}_{\beta}), \quad \tau' \neq \tau,$$

where the constant factors are exactly the same as in (2.26).

The lattice sums $\sigma_{l,m}(\mathbf{k}, \mathbf{s})$ are related to what is also called *structural constants* in some literature [17, 18, 19], but the phase and normalisation differ. For reader's

reference, we list the Ewald-type formulae for lattice sums $\sigma_{l,m}(\mathbf{k}, \mathbf{s})$ rewritten in a way that is independent on particular phase or normalisation conventions of vector spherical harmonics.

In all three lattice dimensionality cases, the lattice sums are divided into short-range and long-range parts, $\sigma_{l,m}(\mathbf{k}, \mathbf{s}) = \sigma_{l,m}^{(S,\eta)}(\mathbf{k}, \mathbf{s}) + \sigma_{l,m}^{(L,\eta)}(\mathbf{k}, \mathbf{s})$ depending on a positive parameter η . The short-range part has in all three cases the same form:

$$(3.8) \quad \sigma_{l,m}^{(S,\eta)}(\mathbf{k}, \mathbf{s}) = -\frac{2^{l+1}i}{\kappa^{l+1}\sqrt{\pi}} \sum_{\mathbf{n} \in \mathbb{Z}^d} (1 - \delta_{\mathbf{R}_n, -\mathbf{s}}) |\mathbf{s}_n|^l Y_{l,m}(\hat{\mathbf{s}}_n) e^{i\mathbf{k} \cdot \mathbf{R}_n} \\ \times \int_{\eta}^{\infty} e^{-|\mathbf{s}_n|^2 \xi^2} e^{-\kappa^2/4\xi^2} \xi^{2l} d\xi \\ + \delta_{\mathbf{R}_n, -\mathbf{s}} \frac{\delta_{l0}\delta_{m0}}{\sqrt{4\pi}} \Gamma\left(-\frac{1}{2}, -\frac{\kappa^2}{4\eta^2}\right) Y_{l,m}(\hat{\mathbf{s}}_n),$$

where we labeled $\mathbf{s}_n \equiv \mathbf{s} + \mathbf{R}_n$. The formal $(1 - \delta_{\mathbf{R}_n, -\mathbf{s}})$ factor here accounts for leaving out the direct excitation of a particle by itself, corresponding to the $(1 - \delta_{\alpha\beta}\delta_{\mathbf{m}\mathbf{0}})$ factor in (3.3). The leaving out then causes an additional (“self-interaction”) term on the last line of (3.8), which appears only when the displacement vector \mathbf{s} coincides with a lattice point. Strictly speaking, this is not a “short-range” term, hence it is often noted separately in the literature; however, we keep it in $\sigma_{l,m}^{(S,\eta)}(\mathbf{k}, \mathbf{s})$ for formal convenience. $\Gamma(a, z)$ is the incomplete Gamma function.

In practice, the integrals in (3.8) can be easily evaluated by numerical quadrature and the incomplete Γ -functions using the series or continued fraction representations from [4].

The explicit form of the long-range part of the lattice sum depends on the lattice dimensionality. The long-range parts are calculated as sums over the reciprocal lattice Λ^* with lattice vectors $\{\mathbf{b}_i\}_{i=1}^d$ lying in the same d -dimensional subspace as the direct lattice vectors $\{\mathbf{a}_i\}_{i=1}^d$ and satisfying $\mathbf{a}_i \cdot \mathbf{b}_j = \delta_{ij}$. In the following, let us label $\mathbf{k}_K \equiv \mathbf{k} + \mathbf{K}$, where \mathbf{K} is a point in the reciprocal lattice, and let \mathcal{A} be the lattice unit cell volume (or area/length in the 2D/1D cases).

Case $d = 3$.

$$(3.9) \quad \sigma_{l,m}^{(L,\eta)}(\mathbf{k}, \mathbf{s}) = \frac{4\pi i^{l+1}}{\kappa \mathcal{A}} \sum_{\mathbf{K} \in \Lambda^*} e^{-i\mathbf{k}_K \cdot \mathbf{s}} \frac{(|\mathbf{k}_K|/\kappa)^l}{\kappa^2 - |\mathbf{k}_K|^2} e^{(\kappa^2 - |\mathbf{k}_K|^2)/4\eta^2} Y_{l,m}(\hat{\mathbf{k}}_K)$$

regardless of chosen coordinate axes. Here \mathcal{A} is the unit cell volume (or length/area in the following 1D/2D lattice cases).

Cases $d = 1, 2$. In the quasiperiodic cases, we decompose vectors into parallel and orthogonal parts with respect to the linear subspace in which the Bravais lattice lies (the reciprocal lattice lies in the same subspace), $\mathbf{v} = \mathbf{v}_{\perp} + \mathbf{v}_{\parallel}$, and we label

$$(3.10) \quad \gamma_{\mathbf{k}_K} \equiv \gamma_{\mathbf{k}_K}(\kappa) \equiv \left(|\mathbf{k}_K|^2 - \kappa^2\right)^{\frac{1}{2}} / \kappa,$$

$$(3.11) \quad \Delta_{d;j}(x, z) \equiv \int_x^{\infty} t^{-\frac{d_c}{2}-n} \exp\left(-t + \frac{z^2}{4t}\right) dt,$$

where $d_c = 3 - d$ is the complementary dimension of the lattice. Then

$$\begin{aligned}
 (3.12) \quad \sigma_l^m(\mathbf{k}, \mathbf{s}) = & \frac{-i}{2\pi^{d_c/2} \mathcal{A}_\kappa} \frac{(2l+1)!!}{\kappa^l} \sum_{\mathbf{K} \in \Lambda^*} e^{-i\mathbf{k}\mathbf{K} \cdot \mathbf{s}} \times \\
 & \times \sum_{j=0}^l \frac{(-1)^j}{j!} \left(\frac{\kappa \gamma_{\mathbf{K}\mathbf{K}}}{2} \right)^{2j} \Delta_{d;j} \left(\frac{\kappa^2 \gamma_{\mathbf{K}\mathbf{K}}^2}{4\eta^2}, -i\kappa \gamma_{\mathbf{K}\mathbf{K}} |\mathbf{s}_\perp| \right) \times \\
 & \times \sum_{l'=\max(0, l-2j)}^{l-j} 4\pi i^{l'} (2|\mathbf{s}_\perp|)^{2j-l+l'} \frac{|\mathbf{k}\mathbf{K}|^{l'}}{(2l'+1)!!} \sum_{m'=-l'}^{l'} Y_{l',m'}(\hat{\mathbf{k}}_{\mathbf{K}}) \times \\
 & \times \int d\Omega_{\mathbf{r}} Y_{l,m}(\hat{\mathbf{r}}) Y_{l',m'}(\hat{\mathbf{r}}) \left(\frac{|\mathbf{r}_\perp|}{|\mathbf{r}|} \right)^{l-l} \left(\frac{-\mathbf{r}_\perp \cdot \mathbf{s}_\perp}{|\mathbf{r}_\perp| |\mathbf{s}_\perp|} \right)^{2j-l+l'}.
 \end{aligned}$$

The angular integral on the last line of (3.12) gives a set of constant coefficients characteristic to a chosen convention for spherical harmonics and coordinate axes; relatively simple closed-form expressions are obtained for 2D periodicity if we choose the lattice to lie in the xy plane, so that both $\mathbf{r}_\perp, \mathbf{s}_\perp$ are parallel to the z axis, as done in [19], see also Supplementary Material. In the special case $\mathbf{s}_\perp = 0$ the expressions can be considerably simplified as most of the terms vanish and $\Delta_{d;j}(x, 0) = \Gamma(1 - d_c/2 - j, x)$, but the general case is needed for evaluating the fields in space (see Section 3.4) or if there is an offset between two particles in a unitcell that is not parallel to the lattice subspace.

If $s_\perp \neq 0$, the integral $\Delta_{d;j}(x, 0)$ can be evaluated e.g. using the Taylor series

$$\Delta_{d;j}(x, z) = \sum_{k=0}^{\infty} \Gamma\left(1 - \frac{d_c}{2} - j - k, x\right) \frac{(z/2)^{2k}}{k!}$$

which has infinite radius of convergence and is the first choice for small z . Kambe [19] mentions a recurrence formula that can be obtained integrating (3.11) by parts (with signs corrected here):

$$(3.13) \quad \Delta_{d;j+1}(x, z) = \frac{4}{z^2} \left(\left(\frac{1}{2} - j \right) \Delta_{d;j}(x, z) - \Delta_{d;j-1}(x, z) + x^{\frac{d_c}{2}-j} e^{-x+\frac{z^2}{4x}} \right)$$

with the first two terms for 2D periodicity

$$\begin{aligned}
 \Delta_{2;0}(x, z) &= \frac{\sqrt{\pi}}{2} e^{-x^2 + \frac{z^2}{4x}} \left(w\left(-\frac{z}{2\sqrt{x}} + i\sqrt{x}\right) + w\left(\frac{z}{2\sqrt{x}} + i\sqrt{x}\right) \right), \\
 \Delta_{2;1}(x, z) &= i \frac{\sqrt{\pi}}{z} e^{-x^2 + \frac{z^2}{4x}} \left(w\left(-\frac{z}{2\sqrt{x}} + i\sqrt{x}\right) - w\left(\frac{z}{2\sqrt{x}} + i\sqrt{x}\right) \right),
 \end{aligned}$$

where $w(z) = e^{-z^2} \left(1 + 2i\pi^{-1/2} \int_0^z e^{t^2} dt \right)$ is the Faddeeva function. However, the recurrence formula (3.13) is unsuitable for numerical evaluation if z is small or j is large due to its numerical instability.

One peculiarity of the two-dimensional case is the two-branchedness of $\gamma_{\mathbf{K}\mathbf{K}}(\kappa)$ and the incomplete Γ -function $\Gamma(\frac{1}{2} - j, z)$ appearing in the long-range part (in the cases $d = 1, 3$ the function $\gamma_{\mathbf{K}\mathbf{K}}(\kappa)$ appears with even powers, and $\Gamma(-j, z)$ is meromorphic for integer j [4, 8.2.9]). As a consequence, if we now explicitly label the dependence on the wavenumber, $\sigma_{l,m}^{(L,\eta)}(\kappa, \mathbf{k}, \mathbf{s})$ has branch points at $\kappa = |\mathbf{k} + \mathbf{K}|$ for every reciprocal lattice vector \mathbf{K} . If the wavenumber κ of the medium has a positive imaginary part, $\Im \kappa > 0$, then the translation operator elements $\mathcal{S}_{\tau lm; \tau' l' m}(\kappa \mathbf{r})$

decay exponentially as $|\mathbf{r}| \rightarrow \infty$ and the lattice sum in (3.3) converges absolutely even in the direct space, and it is equal to the Ewald sum with the principal branches used both in $\gamma(z)$ and $\Gamma(\frac{1}{2} - j, z)$ [26]. For other values of κ , we typically choose the branch in such way that $W_{\alpha\beta}(\mathbf{k})$ is analytically continued even when the wavenumber's imaginary part crosses the real axis. The principal value of $\Gamma(\frac{1}{2} - j, z)$ has a branch cut at the negative real half-axis, which, considering the lattice sum as a function of κ , translates into branch cuts starting at $\kappa = |\mathbf{k} + \mathbf{K}|$ and continuing in straight lines towards $+\infty$. Therefore, in the quadrant $\Re z < 0, \Im z \geq 0$ we use the continuation of the principal value from $\Re z < 0, \Im z < 0$ instead of the principal branch [4, 8.2.9], moving the branch cut in the z variable to the positive imaginary half-axis. This moves the branch cuts w.r.t. κ away from the real axis, as illustrated in Fig. 3.1.

3.3.1. Choice of Ewald parameter and high-frequency breakdown. The Ewald parameter η determines the pace of convergence of both parts. The larger η is, the faster $\sigma_{l,m}^{(S,\eta)}(\mathbf{k}, \mathbf{s})$ converges but the slower $\sigma_{l,m}^{(L,\eta)}(\mathbf{k}, \mathbf{s})$ converges. Therefore (based on the lattice geometry) it has to be adjusted in a way that a reasonable amount of terms needs to be evaluated numerically from both $\sigma_{l,m}^{(S,\eta)}(\mathbf{k}, \mathbf{s})$ and $\sigma_{l,m}^{(L,\eta)}(\mathbf{k}, \mathbf{s})$. For one-dimensional, square, and cubic lattices, the optimal choice for small frequencies (wavenumbers) is $\eta = \sqrt{\pi}/p$ where p is the direct lattice period [26]. However, in floating point arithmetics, the magnitude of the summands must be taken into account as well in order to maintain accuracy.

There is a particular problem with the “central” reciprocal lattice points in the long-range sums for which the real part of $|\mathbf{k}_\mathbf{K}|^2 - \kappa^2$ is negative: the incomplete Γ function present in the sum (either explicitly or in the expansions of Δ_j) grows exponentially with respect to the negative second argument, with asymptotic behaviour $\Gamma(a, z) \sim e^{-z} z^{a-1}$. Therefore for higher frequencies, the parameter η needs to be adjusted in a way that keeps the value of $\Gamma\left(a, \left(|\mathbf{k}_\mathbf{K}|^2 - \kappa^2\right)/4\eta^2\right)$ within reasonable bounds. If we assume that \mathbf{k} lies in the first Brillouin zone, the minimum real part of the second argument of the Γ function will be $\left(|\mathbf{k}|^2 - \kappa^2\right)/4\eta^2$, so setting

$\eta \geq \sqrt{|\kappa|^2 - |\mathbf{k}|^2}/2 \log M$ eliminates the exponential growth in the incomplete Γ function, where the constant M is chosen to represent the (rough) maximum tolerated magnitude of the summand with regard to target accuracy. This adjustment means that, in the worst-case scenario, with growing wavenumber one has to include an increasing number of terms in the long-range sum in order to achieve a given accuracy, the number of terms being proportional to $|\kappa|^d$ where d is the dimension of the lattice.

3.4. Scattering cross sections and field intensities in periodic system.

Once the scattering (3.4) or mode problem (3.5) is solved, one can evaluate some useful related quantities, such as scattering cross sections (coefficients) or field intensities.

For plane wave scattering on 2D lattices, one can directly use the formulae (2.33), (2.36), taking the sums over scatterers inside one unit cell, to get the extinction and absorption cross sections per unit cell. From these, quantities such as absorption, extinction and scattering coefficients are obtained using suitable normalisation by unit cell size, depending on lattice dimensionality.

Ewald summation can be used for evaluating scattered field intensities outside scatterers' circumscribing spheres: this requires expressing VSWF cartesian components in terms of scalar spherical wavefunctions defined in (3.6). Fortunately, these can be obtained easily from the expressions for the translation operator:

$$(3.14) \quad \begin{aligned} \mathbf{v}_{\tau lm}(\kappa \mathbf{r}) &= \sum_{m'=-1}^1 \mathcal{R}_{\tau lm;21m'}(\kappa \mathbf{r}) \mathbf{v}_{21m'}(0), \\ \mathbf{u}_{\tau lm}(\kappa \mathbf{r}) &= \sum_{m'=-1}^1 \mathcal{S}_{\tau lm;21m'}(\kappa \mathbf{r}) \mathbf{v}_{21m'}(0), \end{aligned}$$

which follows from eqs. (2.18), (2.19) and the fact that all the other regular VSWFs except for $\mathbf{v}_{21m'}$ vanish at origin. For the quasiperiodic scattering problem formulated in section 3.1, the total electric field scattered from all the particles at point \mathbf{r} located outside all the particles' circumscribing sphere reads, using eqs. (2.25), (3.7), (3.6),

$$(3.15) \quad \begin{aligned} \mathbf{E}_{\text{scat}}(\mathbf{r}) &= \sum_{(\mathbf{n}, \alpha) \in \mathcal{P}} \sum_{\tau lm} f_{\mathbf{n}, \alpha, \tau lm} \mathbf{u}_{\tau lm}(\kappa(\mathbf{r} - \mathbf{R}_{\mathbf{n}} - \mathbf{r}_{\alpha})) = \\ &= \sum_{\alpha \in \mathcal{P}_1} \sum_{\tau lm} f_{\mathbf{0}, \alpha, \tau lm} \sum_{m'=-1}^1 \mathbf{v}_{21m'}(0) \sum_{\lambda=|l-1|+|\tau-2|}^{l+1} C_{\tau lm;21m'}^{\lambda} \sigma_{\lambda, m-m'}(-\mathbf{k}, \mathbf{r} - \mathbf{r}_{\alpha}). \end{aligned}$$

In the scattering problem, the total field intensity is obtained by adding the incident field to (3.15); whereas in the lattice mode problem the total field is directly given by (3.15).

4. SYMMETRIES

If the system has nontrivial point group symmetries, group theory gives additional understanding of the system properties, and can be used to substantially reduce the computational costs.

As an example, if the system has a D_{2h} symmetry and the corresponding truncated $(I - TS)$ matrix has size $N \times N$, it can be block-diagonalized into eight blocks of size about $N/8 \times N/8$, each of which can be LU-factorised separately (this is due to the fact that D_{2h} has eight different one-dimensional irreducible representations). This can reduce both memory and time requirements to solve the scattering problem (2.17) by a factor of 64.

In periodic systems (problems (3.4), (3.5)) due to small number of particles per unit cell, the costliest part is usually the evaluation of the lattice sums in the $W(\omega, \mathbf{k})$ matrix, not the linear algebra. However, decomposition of the lattice mode problem (3.5) into the irreducible representations of the corresponding little co-groups of the system's space group is nevertheless a useful tool in the mode analysis: among other things, it enables separation of the lattice modes (which can then be searched for each irrep separately), and the irrep dimension gives a priori information about mode degeneracy.

4.1. Excitation coefficients under point group operations. In order to make use of the point group symmetries, we first need to know how they affect our basis functions, i.e. the VSWFs. Let g be a member of the orthogonal group $O(3)$, i.e. a 3D point rotation or reflection operation that transforms vectors in \mathbb{R}^3 with an orthogonal matrix R_g :

$$\mathbf{r} \mapsto R_g \mathbf{r}.$$

With \hat{P}_g we shall denote the action of g on a field in real space. For a scalar field w we have $(\hat{P}_g w)(\mathbf{r}) = w(R_g^{-1} \mathbf{r})$, whereas for a vector field \mathbf{w} , $(\hat{P}_g \mathbf{w})(\mathbf{r}) = R_g \mathbf{w}(R_g^{-1} \mathbf{r})$.

Spherical harmonics $Y_{l,m}$, being a basis of the l -dimensional representation of $O(3)$, transform as [56, Chapter 15]

$$(4.1) \quad (\hat{P}_g Y_{l,m})(\hat{\mathbf{r}}) = Y_{l,m}(R_g^{-1} \hat{\mathbf{r}}) = \sum_{m'=-l}^l D_{m,m'}^l(g) Y_{l,m'}(\hat{\mathbf{r}})$$

where $D_{m,m'}^l(g)$ denotes the elements of the *Wigner matrix* representing the operation g . From their definitions (2.4) and the properties of the gradient operator under coordinate transforms, vector spherical harmonics $\mathbf{A}_{2,l,m}, \mathbf{A}_{3,l,m}$ transform in the same way,

$$\begin{aligned} (\hat{P}_g \mathbf{A}_{2,l,m})(\hat{\mathbf{r}}) &= \sum_{m'=-l}^l D_{m,m'}^l(g) \mathbf{A}_{2,l,m'}(\hat{\mathbf{r}}), \\ (\hat{P}_g \mathbf{A}_{3,l,m})(\hat{\mathbf{r}}) &= \sum_{m'=-l}^l D_{m,m'}^l(g) \mathbf{A}_{3,l,m'}(\hat{\mathbf{r}}), \end{aligned}$$

but the remaining set $\mathbf{A}_{1,l,m}$ transforms differently due to their pseudovector nature stemming from the cross product in their definition:

$$\left(\hat{P}_g \mathbf{A}_{1,l,m}\right)(\hat{\mathbf{r}}) = \sum_{m'=-l}^l \widetilde{D_{m,m'}^l}(g) \mathbf{A}_{1,l,m'}(\hat{\mathbf{r}}),$$

where $\widetilde{D_{m,m'}^l}(g) = D_{m,m'}^l(g)$ if g is a proper rotation, $g \in \text{SO}(3)$, but for spatial inversion operation $i : \mathbf{r} \mapsto -\mathbf{r}$ we have $D_{m,m'}^l(i) = (-1)^l$ but $\widetilde{D_{m,m'}^l}(i) = (-1)^{l+1}$. The transformation behaviour of vector spherical harmonics directly propagates to vector spherical waves, cf. (2.2), (2.3):

$$\begin{aligned} \left(\hat{P}_g \mathbf{u}_{1lm}\right)(\mathbf{r}) &= \sum_{m'=-l}^l \widetilde{D_{m,m'}^l}(g) \mathbf{u}_{1lm'}(\mathbf{r}), \\ \left(\hat{P}_g \mathbf{u}_{2lm}\right)(\mathbf{r}) &= \sum_{m'=-l}^l D_{m,m'}^l(g) \mathbf{u}_{2lm'}(\mathbf{r}), \end{aligned}$$

and analogously for the regular waves $\mathbf{v}_{\tau lm}$. For convenience, we introduce the symbol $D_{m,m'}^{\tau l}$ that describes the transformation of both (“magnetic” and “electric”) types of waves at once:

$$\hat{P}_g \mathbf{u}_{\tau lm}(\mathbf{r}) = \sum_{m'=-l}^l D_{m,m'}^{\tau l}(g) \mathbf{u}_{\tau lm'}(\mathbf{r}).$$

Note that this symbol retains the unitarity of the original Wigner matrices,

$$(4.2) \quad \sum_{m'} (D_{m,m'}^{\tau l}(g))^* D_{\mu,m'}^{\tau l}(g) = \delta_{m\mu}.$$

Using these, we can express the VSWF expansion (2.7) of the electric field around origin in a rotated/reflected system,

$$(4.3) \quad \left(\hat{P}_g \mathbf{E}\right)(\omega, \mathbf{r}) = \sum_{\tau=1,2} \sum_{l=1}^{\infty} \sum_{m=-l}^{+l} \sum_{m'=-l}^l \left(a_{\tau lm} D_{m,m'}^{\tau l}(g) \mathbf{v}_{\tau lm'}(\kappa \mathbf{r}) + f_{\tau lm} D_{m,m'}^{\tau l}(g) \mathbf{u}_{\tau lm'}(\kappa \mathbf{r}) \right),$$

which, together with the T -matrix definition, (2.8) can be used to obtain a T -matrix of a rotated or mirror-reflected particle. Let T be the T -matrix of an original particle; the T -matrix of a particle physically transformed by operation $g \in O(3)$ is then (following from eqs. (4.3), (2.8), (4.2))

$$(4.4) \quad T'_{\tau lm; \tau' l' m'} = \sum_{\mu=-l}^l \sum_{\mu'=-l'}^{l'} D_{\mu,m}^{\tau l}(g) T_{\tau l \mu; \tau' l' \mu'} \left(D_{\mu',m'}^{\tau' l'}(g) \right)^*.$$

If the particle is symmetric (so that g produces a particle indistinguishable from the original one), the T -matrix must remain invariant under the transformation (4.4), $T'_{\tau lm; \tau' l' m'} = T_{\tau lm; \tau' l' m'}$. Explicit forms of these invariance properties for the most important point group symmetries can be found in [45].

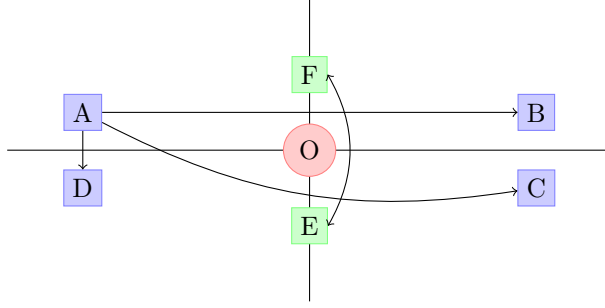


FIGURE 4.1. Scatterer orbits under D_2 symmetry. Particles A, B, C, D lie outside of origin or any mirror planes, and together constitute an orbit of the size equal to the order of the group, $|D_2| = 4$. Particles E, F lie on the yz plane, hence the corresponding reflection maps each of them to itself, but the xz reflection (or the π rotation around the z axis) maps them to each other, forming a particle orbit of size 2. The particle O in the very origin is always mapped to itself, constituting its own orbit.

If the field expansion is done around a point \mathbf{r}_p different from the global origin, as in 2.14, we have

(4.5)

$$\begin{aligned} \left(\hat{P}_g \mathbf{E}\right)(\omega, \mathbf{r}) = & \sum_{\tau=1,2} \sum_{l=1}^{\infty} \sum_{m=-l}^{+l} \sum_{m'=-l}^l (a_{p,\tau lm} D_{m,m'}^{\tau l}(g) \mathbf{v}_{\tau lm'}(\kappa(\mathbf{r} - R_g \mathbf{r}_p)) + \\ & + f_{p,\tau lm} D_{m,m'}^{\tau l}(g) \mathbf{u}_{\tau lm'}(\kappa(\mathbf{r} - R_g \mathbf{r}_p))) . \end{aligned}$$

With these transformation properties in hand, we can proceed to the effects of point symmetries on the whole many-particle system. Let us have a many-particle system symmetric with respect to a point group G . A symmetry operation $g \in G$ determines a permutation of the particles: $p \mapsto \pi_g(p)$, $p \in \mathcal{P}$; their positions transform as $\mathbf{r}_{\pi_g p} = R_g \mathbf{r}_p$, $\mathbf{r}_{\pi_g^{-1} p} = R_g^{-1} \mathbf{r}_p$. In the symmetric multiple-scattering problem, transforming the whole field according to g , in terms of field expansion around a particle originally labelled as p

$$\begin{aligned} \left(\hat{P}_g \mathbf{E}\right)(\omega, \mathbf{r}) = & \sum_{\tau=1,2} \sum_{l=1}^{\infty} \sum_{m=-l}^{+l} \sum_{m'=-l}^l (a_{p,\tau lm} D_{m,m'}^{\tau l}(g) \mathbf{v}_{\tau lm'}(\kappa(\mathbf{r} - R_g \mathbf{r}_p)) + \\ & + f_{p,\tau lm} D_{m,m'}^{\tau l}(g) \mathbf{u}_{\tau lm'}(\kappa(\mathbf{r} - R_g \mathbf{r}_p))) \\ = & \sum_{\tau=1,2} \sum_{l=1}^{\infty} \sum_{m=-l}^{+l} \sum_{m'=-l}^l (a_{p,\tau lm} D_{m,m'}^{\tau l}(g) \mathbf{v}_{\tau lm'}(\kappa(\mathbf{r} - \mathbf{r}_{\pi_g p})) \\ & + f_{p,\tau lm} D_{m,m'}^{\tau l}(g) \mathbf{u}_{\tau lm'}(\kappa(\mathbf{r} - \mathbf{r}_{\pi_g p}))) \\ = & \sum_{\tau=1,2} \sum_{l=1}^{\infty} \sum_{m=-l}^{+l} \sum_{m'=-l}^l \left(a_{\pi_g^{-1} q, \tau lm} D_{m,m'}^{\tau l}(g) \mathbf{v}_{\tau lm'}(\kappa(\mathbf{r} - \mathbf{r}_q)) \right. \\ & \left. + f_{\pi_g^{-1} q, \tau lm} D_{m,m'}^{\tau l}(g) \mathbf{u}_{\tau lm'}(\kappa(\mathbf{r} - \mathbf{r}_q)) \right) . \end{aligned}$$

In the last step, we relabeled $q = \pi_g p$. This means that the field expansion coefficients a_p, f_p transform as

$$(4.6) \quad \begin{aligned} a_{p,\tau l m'} &\xrightarrow{g} \sum_{m=-l}^l a_{\pi_g^{-1}(p),\tau l m} D_{m,m'}^{\tau l}(g), \\ f_{p,\tau l m'} &\xrightarrow{g} \sum_{m=-l}^l f_{\pi_g^{-1}(p),\tau l m} D_{m,m'}^{\tau l}(g). \end{aligned}$$

For a given particle p , we will call the set of particles onto which any of the symmetries maps the particle p , i.e. the set $\{\pi_g(p); g \in G\}$, as the *orbit* of particle p . The whole set \mathcal{P} can therefore be divided into the different particle orbits; an example is in Fig. 4.1. The importance of the particle orbits stems from fact that the expansion coefficients belonging to particles in different orbits are not related together under the group action in (4.6). As before, we introduce a short-hand pairwise matrix notation for (4.6)

$$(4.7) \quad \begin{aligned} a_p &\xrightarrow{g} \tilde{J}(g) a_{\pi_g^{-1}(p)}, \\ f_p &\xrightarrow{g} \tilde{J}(g) f_{\pi_g^{-1}(p)}, \end{aligned}$$

and also a global block-matrix form

$$(4.8) \quad \begin{aligned} a &\xrightarrow{g} J(g) a, \\ f &\xrightarrow{g} J(g) f. \end{aligned}$$

If the particle indices are ordered in a way that the particles belonging to the same orbit are grouped together, $J(g)$ will be a block-diagonal unitary matrix, each block (also unitary) representing the action of g on one particle orbit. All the $J(g)$ s make together a (reducible) linear representation of G .

4.2. Irrep decomposition. Knowledge of symmetry group actions $J(g)$ on the field expansion coefficients give us the possibility to construct a symmetry adapted basis in which we can block-diagonalise the multiple-scattering problem matrix $(I - TS)$. Let Γ_n be the d_n -dimensional irreducible matrix representations of G consisting of matrices $D^{\Gamma_n}(g)$. Then the projection operators

$$P_{kl}^{(\Gamma_n)} \equiv \frac{d_n}{|G|} \sum_{g \in G} (D^{\Gamma_n}(g))_{kl}^* J(g), \quad k, l = 1, \dots, d_n$$

project the full scattering system field expansion coefficient vectors a, f onto a subspace corresponding to the irreducible representation Γ_n . The projectors can be used to construct a unitary transformation U with components

$$(4.9) \quad U_{nri;p\tau lm} = \frac{d_n}{|G|} \sum_{g \in G} (D^{\Gamma_n}(g))_{rr'}^* J(g)_{p'\tau' l' m' (nri); p\tau lm}$$

where r goes from 1 to d_n and i goes from 1 to the multiplicity of irreducible representation Γ_n in the (reducible) representation of G spanned by the field expansion coefficients a or f . The indices p', τ', l', m' are given by an arbitrary bijective mapping $(n, r, i) \mapsto (p', \tau', l', m')$ with the constraint that for given n, r, i there are at least some non-zero elements $U_{nri;p\tau lm}$. For details, we refer the reader to textbooks about group representation theory, e.g. [5, Chapter 4] or [2, Chapter 2]. The

transformation given by U transforms the excitation coefficient vectors a, f into a new, *symmetry-adapted basis*.

One can show that if an operator M acting on the excitation coefficient vectors is invariant under the operations of group G , meaning that

$$\forall g \in G : J(g) M J(g)^\dagger = M,$$

then in the symmetry-adapted basis, M is block diagonal, or more specifically

$$M_{\Gamma, r, i; \Gamma', r', j}^{\text{s.a.b.}} = \frac{\delta_{\Gamma \Gamma'} \delta_{ij}}{d_\Gamma} \sum_q M_{\Gamma, r, q; \Gamma', r', q}^{\text{s.a.b.}}$$

Both the T and \mathcal{S} operators (and trivially also the identity I) in (2.17) are invariant under the actions of whole system symmetry group, so $(I - T\mathcal{S})$ is also invariant, hence $U(I - T\mathcal{S})U^\dagger$ is a block-diagonal matrix, and the problem (2.17) can be solved for each block separately.

From the computational perspective, it is important to note that U is at least as sparse as $J(g)$ (which is “orbit-block” diagonal), hence the block-diagonalisation can be performed fast.

4.3. Periodic systems. Also for periodic systems, $M(\omega, \mathbf{k}) = (I - T(\omega)W(\omega, \mathbf{k}))$ from the left hand side of eqs. (3.4), (3.5) can be block-diagonalised in a similar manner. However, in this case, $W(\omega, \mathbf{k})$ is in general not invariant under the whole point group symmetry subgroup of the system geometry due to the \mathbf{k} dependence. In other words, only those point symmetries that the $e^{i\mathbf{k}\cdot\mathbf{r}}$ modulation does not break are preserved, and no preservation of point symmetries happens unless \mathbf{k} lies somewhere in the high-symmetry parts of the Brillouin zone. However, the high-symmetry points are usually the ones of the highest physical interest, for it is where the band edges are typically located. This subsection does not aim for an exhaustive treatment of the topic of space groups in physics (which can be found elsewhere [5, 2]), here we rather demonstrate how the group action matrices are generated on a specific example of a symmmorphic space group.

The transformation to the symmetry adapted basis U is constructed in a similar way as in the finite case, but because we do not work with all the (infinite number of) scatterers but only with one unit cell, additional phase factors $e^{i\mathbf{k}\cdot\mathbf{r}_p}$ appear in the per-unit-cell group action $J(g)$: this can happen if the point group symmetry maps some of the scatterers from the reference unit cell to scatterers belonging to other unit cells. This is illustrated in Fig. 4.2. Fig. 4.2a shows a hexagonal periodic array with $p6m$ wallpaper group symmetry, with lattice vectors $\mathbf{a}_1 = (a, 0)$ and $\mathbf{a}_2 = (a/2, \sqrt{3}a/2)$. We delimit our representative unit cell as the Wigner-Seitz cell with origin in a D_6 point group symmetry center (there is one per each unit cell); per unit cell, there are five different particles placed on the unit cell boundary, and we need to make a choice to which unit cell the particles on the boundary belong; in our case, we choose that a unit cell includes the particles on the left as denoted by different colors. If the Bloch vector is at the upper M point, $\mathbf{k} = \mathbf{M}_1 = (0, 2\pi/\sqrt{3}a)$, it creates a relative phase of π between the unit cell rows, and the original D_6 symmetry is reduced to D_2 . The “horizontal” mirror operation σ_{xz} maps, according to our boundary division, all the particles only inside the same

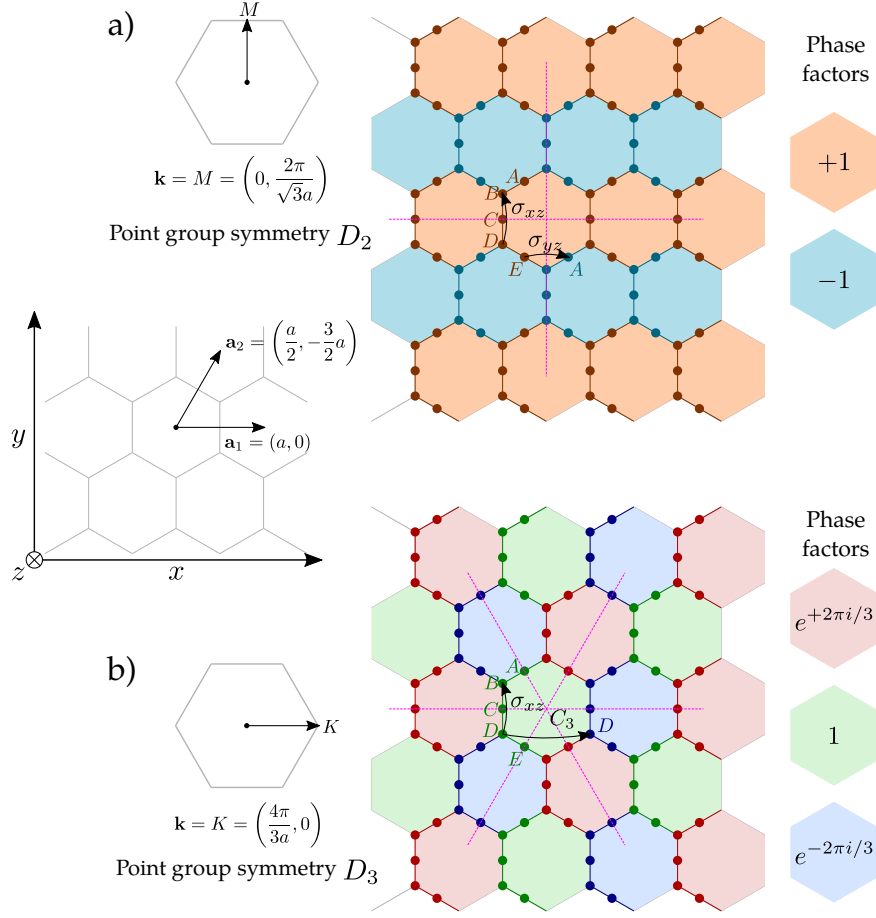


FIGURE 4.2. Representing symmetry action on electromagnetic Bloch waves in a lattice with $p6m$ wallpaper group symmetry. In a hexagonal array with five particles (labeled $A-E$) per unit cell, we first choose into which unit cells do the particles on unit cell boundaries belong. a) At M point, the little co-group contains a D_2 point group; the unit cells can be divided into two groups (alternating horizontal rows) with opposite sign. The horizontal mirror operation σ_{xz} maps the particles from a single unit cell to each other. However, the vertical mirror operation σ_{yz} maps them onto particles belonging to different unit cells, introducing possible phase factors in the point group action: B, C, D map onto B, C, D belonging to different unit cell from same phase group, so no additional phase is needed; however, A, E map onto E, A belonging to unitcells with relative phases $\pm\pi$, therefore the corresponding action matrix blocks will carry a factor -1 . b) At K point point, little co-group contains a D_3 point group, and the unit cells divide into three groups with relative phase shift $e^{2\pi i/3}$. The horizontal mirroring σ_{xz} again does not introduce any additional phase. However, the C_3 rotation mixes particles belonging to different unit cells, so for example particle D maps onto particle D , but with additional phase factor $e^{-2\pi i/3}$.

unit cell, e.g.

$$\begin{aligned} f_{0A} &\xrightarrow{\sigma_{xz}} \tilde{J}(\sigma_{xz}) f_{0E}, \\ f_{0C} &\xrightarrow{\sigma_{xz}} \tilde{J}(\sigma_{xz}) f_{0C}, \end{aligned}$$

as in eq. (4.6). However, both the “vertical” mirroring σ_{yz} and the C_2 rotation map the boundary particles onto the boundaries that do not belong to the reference unit cell with $\mathbf{n} = (0, 0)$, so we have, explicitly writing down also the lattice point indices \mathbf{n} ,

$$\begin{aligned} f_{0A} &\xrightarrow{\sigma_{yz}} \tilde{J}(\sigma_{yz}) f_{(0,1)E}, \\ f_{0C} &\xrightarrow{\sigma_{yz}} \tilde{J}(\sigma_{yz}) f_{(1,0)C}, \end{aligned}$$

but we want $J(g)$ to operate only inside one unit cell, so we use the Bloch condition $f_{\mathbf{n},\alpha} = f_{0,\alpha}(\mathbf{k}) e^{i\mathbf{k}\cdot\mathbf{R}\cdot\mathbf{n}}$: in this case, we have $f_{(0,1)\alpha} = f_{0\alpha} e^{i\mathbf{M}_1\cdot\mathbf{a}_2} = f_{0\alpha} e^{i0} = f_{0\alpha}$, $f_{(1,0)\alpha} = e^{i\mathbf{M}_1\cdot\mathbf{a}_2} f_{0\alpha} = e^{i\pi} f_{0\alpha} = -f_{0\alpha}$, so

$$\begin{aligned} f_{0A} &\xrightarrow{\sigma_{yz}} -\tilde{J}(\sigma_{yz}) f_{0E}, \\ f_{0C} &\xrightarrow{\sigma_{yz}} \tilde{J}(\sigma_{yz}) f_{0C}. \end{aligned}$$

If we set instead $\mathbf{k} = \mathbf{K} = (4\pi/3a, 0)$, the original D_6 point group symmetry reduces to D_3 and the unit cells can obtain a relative phase factor of $e^{-2\pi i/3}$ (blue) or $e^{2\pi i/3}$ (red). The σ_{xz} mirror symmetry, as in the previous case, acts purely inside the reference unit cell with our boundary division. However, for a counterclockwise C_3 rotation as an example we have (see Fig. 4.2b)

$$\begin{aligned} f_{0A} &\xrightarrow{C_3} \tilde{J}(C_3) f_{(0,-1)E} = e^{2\pi i/3} \tilde{J}(C_3) f_{0E}, \\ f_{0C} &\xrightarrow{C_3} \tilde{J}(C_3) f_{(1,-1)A} = e^{-2\pi i/3} \tilde{J}(C_3) f_{0A}, \\ f_{0B} &\xrightarrow{C_3} \tilde{J}(C_3) f_{(1,-1)B} = e^{-2\pi i/3} \tilde{J}(C_3) f_{0B}, \end{aligned}$$

because in this case, the Bloch condition gives $f_{(0,-1)\alpha} = f_{0\alpha} e^{i\mathbf{K}\cdot(-\mathbf{a}_2)} = f_{0\alpha} e^{-4\pi i/3} = f_{0\alpha} e^{2\pi i/3} = f_{0\alpha}$, $f_{(1,-1)\alpha} = f_{0\alpha} e^{i\mathbf{K}\cdot(\mathbf{a}_1-\mathbf{a}_2)} = e^{-2\pi i/3} f_{0\alpha}$.

Having the group action matrices, we can construct the projectors and decompose the system into irreducible representations of the corresponding point groups analogously to the finite case (4.9). This procedure can be repeated for any system with a symmorphic space group symmetry, where the translation and point group operations are essentially separable. For systems with non-symmorphic space group symmetries (i.e. those with glide reflection planes or screw rotation axes) a more refined approach is required [2, 5].

5. APPLICATIONS

Finally, we present some results obtained with the QPMS suite. Scripts to reproduce these results are available under the `examples` directory of the QPMS source repository.

For further results, used for explaining experiments, see Refs. [11] (scattering, finite system), [10, 37] (approximate lattice mode search using a real-frequency-only scan), and [51] (resonances of a finite system). Note that in [11, 10], T -matrices were calculated using a buggy version of SCUFF-EM.

5.1. Optical response of a square array; finite size effects. Our first example deals with a plasmonic array made of silver nanoparticles placed in a square planar configuration. The nanoparticles have shape of right circular cylinder with 30 nm radius and 30 nm in height. The particles are placed with periodicity $p_x = p_y = 375$ nm into an isotropic medium with a constant refraction index $n = 1.52$. For silver, we use Drude-Lorentz model with parameters from [39], and the T -matrix of a single particle we compute using the null-field method (with cutoff $l_{\max} = 6$ for solving the null-field equations).

We consider finite arrays with $N_x \times N_y = 40 \times 40, 70 \times 70, 100 \times 100$ particles and also the corresponding infinite array, and simulate their absorption when irradiated by plane waves with incidence direction lying in the xz plane. We concentrate on the behaviour around the first diffracted order crossing at the Γ point, which happens around frequency $2.18 \text{ eV}/\hbar$. Figure 5.1 shows the response for the infinite array for a range of frequencies; here in particular we used the multipole cutoff $l_{\max} = 3$ for the interparticle interactions, although there is no visible difference if we use $l_{\max} = 2$ instead due to the small size of the particles. In Figure 5.2, we compare the response of differently sized array slightly below the diffracted order crossing. We see that far from the diffracted orders, all the cross sections are almost directly proportional to the total number of particles. However, near the resonances, the size effects become apparent: the lattice resonances tend to fade away as the size of the array decreases. Moreover, the proportion between the absorbed and scattered parts changes as while the small arrays tend to more just scatter the incident light into different directions, in larger arrays, it is more “likely” that the light will scatter many times, each time sacrificing a part of its energy to the ohmic losses.

The finite-size cases in Figure 5.2 were computed with quadrupole truncation $l \leq 2$ and using the decomposition into the eight irreducible representations of group D_{2h} . The 100×100 array took about 4 h to compute on Dell PowerEdge C4130 with 12 core Xeon E5 2680 v3 2.50GHz, requiring about 20 GB of RAM. For smaller systems, the computation time decreases quickly, as the main bottleneck is the LU factorisation. In any case, there is still room for optimisation in the QPMS suite.

5.2. Lattice mode structure of a square lattice. Next, we study the lattice mode problem of the same square arrays. First we consider the mode problem exactly at the Γ point, $\mathbf{k} = 0$. Before proceeding with more sophisticated methods, it is often helpful to look at the singular values of mode problem matrix $M(\omega, \mathbf{k})$ from the lattice mode equation (3.5), as shown in Fig. 5.3. This can be always done, even with tabulated/interpolated material properties and/or T -matrices. An additional insight, especially in the high-symmetry points of the Brillouin zone, is provided by decomposition of the matrix into irreps – in this case of group D_{4h} ,

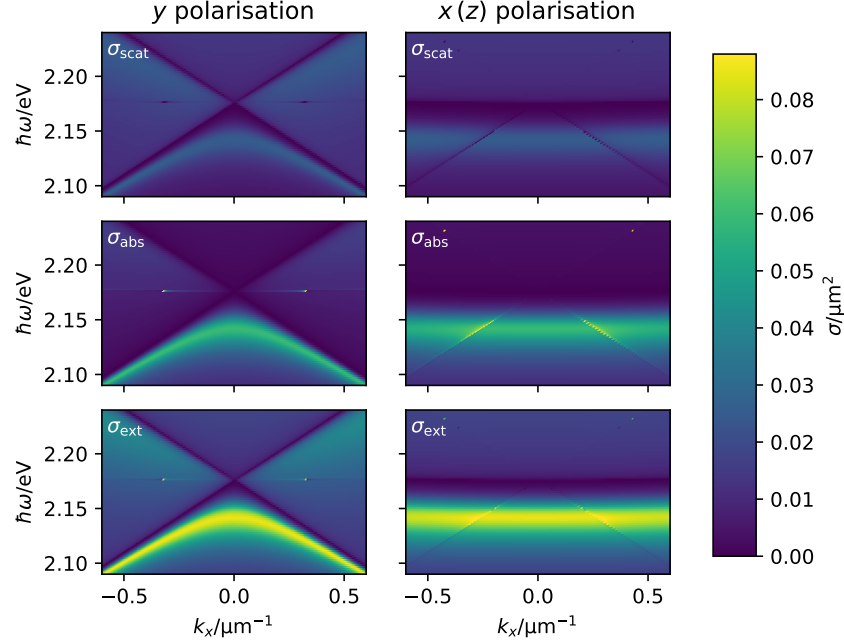


FIGURE 5.1. Response of an infinite square array of silver nanoparticles with periodicities $p_x = p_y = 375$ nm to plane waves incident in the xz -plane, with y -polarised waves (left), and x -polarised waves (right). The images show extinction, scattering and absorption cross section per unit cell.

which corresponds to the point group symmetry of the array at the Γ point. Although on the picture none of the SVDs hits manifestly zero, we see two prominent dips in the E' and A_2'' irrep subspaces, which is a sign of an actual solution nearby in the complex plane. Moreover, there might be some less obvious minima in the very vicinity of the diffracted order crossing which do not appear in the picture due to rough frequency sampling.

As we have used only analytical ingredients in $M(\omega, \mathbf{k})$, the matrix is itself analytical, hence Beyn's algorithm can be used to search for complex mode frequencies, which is shown in Figure 5.4. The number of the frequency point found is largely dependent on the parameters used in Beyn's algorithm, mostly the integration contour in the frequency space. Here we used ellipses discretised by 250 points each, with edges nearly touching the empty lattice diffracted orders (from either above or below in the real part), and with major axis covering $1/5$ of the interval between two diffracted orders. The residual threshold was set to 0.1. At the Γ point, the algorithm finds the actual complex positions of the suspected E' and A_2'' modes without a problem, as well as their continuations to the other nearby values of \mathbf{k} . However, for further \mathbf{k} it might "lose track", especially as the modes cross the diffracted orders. As a result, the parameters of Beyn's algorithm often require manual tuning based on the observed behaviour.

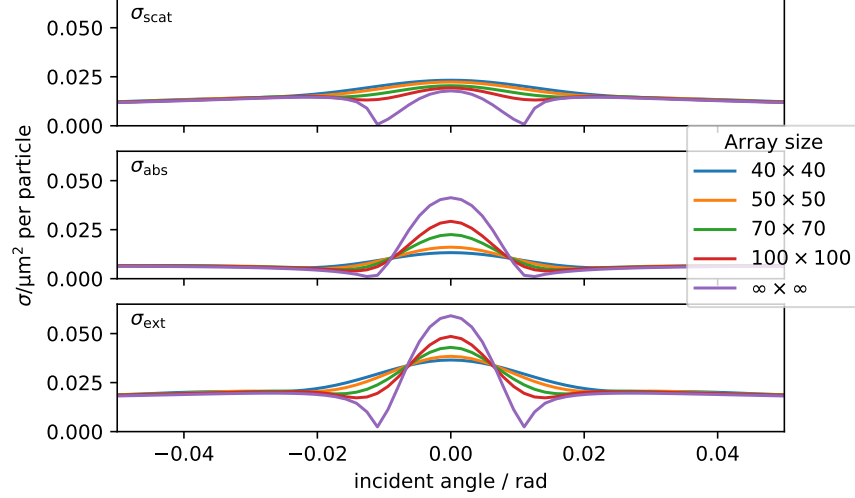


FIGURE 5.2. Comparison of optical responses of differently sized square arrays of silver nanoparticles with the same periodicity $p_x = p_y = 375$ nm. In all cases, the array is illuminated by plane waves linearly polarised in the y -direction, with constant frequency 2.15 eV/ \hbar . The cross sections are normalised by the total number of particles in the array.

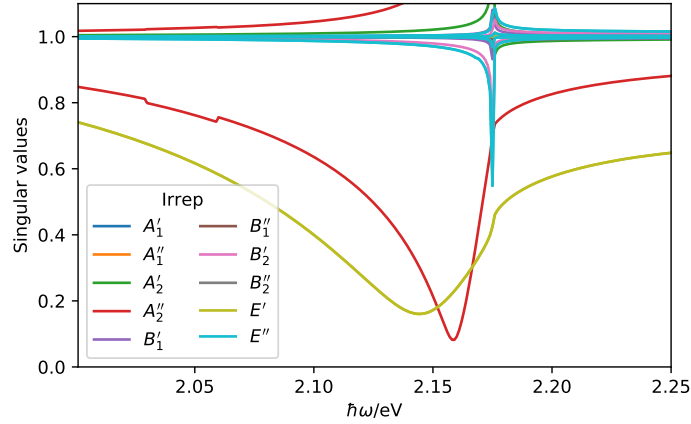


FIGURE 5.3. Singular values of the mode problem matrix $[M(\omega, \mathbf{k} = 0)]_{l \leq 3}$ for a real frequency interval. The irreducible representations of D_{4h} are labeled with different colors. The density of the data points on the horizontal axis is $1/\text{meV}$.

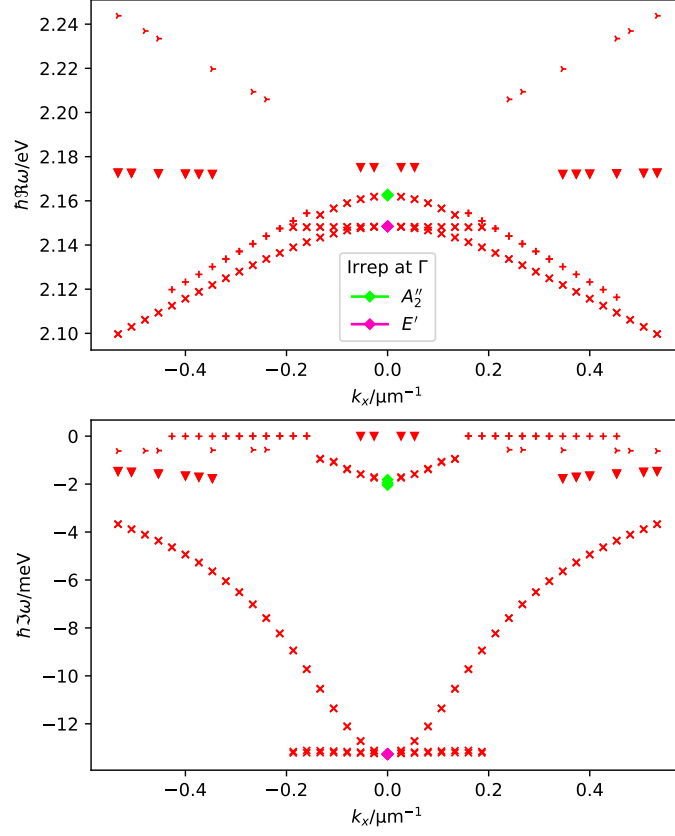


FIGURE 5.4. Solutions of the lattice mode problem $[M(\omega, \mathbf{k})]_{l \leq 3}$ found using the Beyn's method near the first diffracted order crossing at the Γ point for $k_y = 0$. At the Γ point, they are classified according to the irreducible representations of D_{4h} .

5.3. Effects of multipole cutoff. In order to demonstrate some of the consequences of multipole cutoff, we consider a square lattice with periodicity $p_x = p_y = 580 \text{ nm}$ filled with spherical golden nanoparticles (with Drude-Lorentz model for permittivity; one sphere per unit cell) embedded in a medium with a constant refractive index $n = 1.52$. We vary the multipole cutoff $l_{\max} = 1, \dots, 5$ and the particle radius $r = 50 \text{ nm}, \dots, 300 \text{ nm}$ (note that right end of this interval is unphysical, as the spheres touch at $r = 290 \text{ nm}$) We look at the lattice modes at the Γ point right below the diffracted order crossing at 1.406 eV using Beyn's algorithm; the integration contour for Beyn's algorithm being a circle with centre at

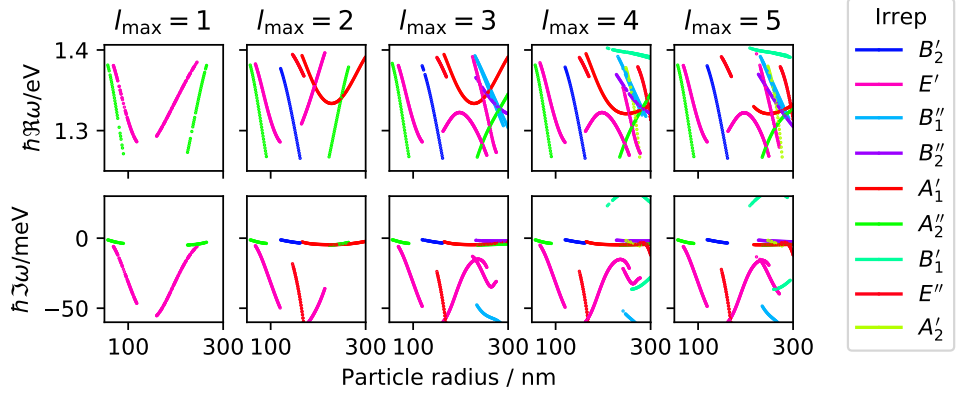


FIGURE 5.5. Consequences of multipole degree cutoff: Eigenfrequencies found with the Beyn's algorithm for an infinite square lattice of golden spherical nanoparticles with varying particle size.

$\omega = (1.335 + 0i) \text{ eV}/\hbar$ and radius $70.3 \text{ meV}/\hbar$, and 410 sample points. We classify each of the found modes as one of the ten irreducible representations of the corresponding little group at the Γ point, D_{4h} .

The real and imaginary parts of the obtained mode frequencies are shown in Fig. 5.5. The most obvious (and expected) effect of the cutoff is the reduction of the number of modes found: the case $l_{\max} = 1$ (dipole-dipole approximation) contains only the modes with nontrivial dipole excitations (x, y dipoles in E' and z dipole in A''_2). For relatively small particle sizes, the main effect of increasing l_{\max} is making the higher multipolar modes accessible at all. As the particle radius increases, there start to appear more non-negligible elements in the T -matrix, and the cutoff then affects the mode frequencies as well.

Another effect related to mode finding is, that increasing l_{\max} leads to overall decrease of the lowest singular values of the mode problem matrix $M(\omega, \mathbf{k})$, so that they are very close to zero for a large frequency area, making it harder to determine the exact roots of the mode equation (3.5), which might lead to some spurious results: Fig. 5.5 shows modes with positive imaginary frequencies for $l_{\max} \geq 3$, which is unphysical (positive imaginary frequency means effective losses of the medium, which, together with the lossy particles, prevent emergence of propagating modes). However, the spurious frequencies can be made disappear by tuning the parameters of Beyn's algorithm (namely, stricter residual threshold), but that might lead to losing legitimate results as well, especially if they are close to the integration contour. In such cases, it is often helpful to run Beyn's algorithm several times with different contours enclosing smaller frequency areas.

6. SUMMARY

We presented two major enhancements of the electromagnetic multiple-scattering T -matrix method: 1) Employing Ewald summation techniques enables very efficient computation of lattice modes and optical response of infinite periodic nanoparticle structures. 2) Exploiting possible symmetries of the system by transformation into symmetry adapted basis reduces the requirements on computational resources considerably, enabling simulations of finite systems with tens of thousands of scatterers. These enhancements are included into the QPMS software suite, which we hereby make publicly available under the GNU General Public License.

7. ACKNOWLEDGMENTS

We thank Nicki Källman, Kristian Arjas, Javier Cuerda and Vadim Zakomirnyi for useful discussions. This work was supported by the Academy of Finland under project numbers 303351, 307419, 327293, 318987 (QuantERA project RouTe), and by the European Research Council (ERC-2013-AdG-340748-CODE). We acknowledge the computational resources provided by the Aalto Science-IT project.

REFERENCES

1. Wolf-Jürgen Beyn, *An integral method for solving nonlinear eigenvalue problems*, Linear Algebra and its Applications **436** (2012), no. 10, 3839–3863.
2. C. J. Bradley and A. P. Cracknell, *The mathematical theory of symmetry in solids; representation theory for point groups and space groups*, Clarendon Press, Oxford, 1972.
3. Krzysztof M. Czajkowski, Maria Bancerek, and Tomasz J. Antosiewicz, *Multipole analysis of substrate-supported dielectric nanoresonator arrays with T -matrix method*, arXiv:2006.09137 [physics] (2020).
4. *NIST Digital Library of Mathematical Functions*, online resource at <http://dlmf.nist.gov/>.
5. Mildred S. Dresselhaus, Gene Dresselhaus, and Ado Jorio, *Group Theory: Application to the Physics of Condensed Matter*, Springer, Berlin, Heidelberg, 2008.
6. P. P. Ewald, *Die Berechnung optischer und elektrostatischer Gitterpotentiale*, Annalen der Physik **369** (1921), no. 3, 253–287 (en).
7. M. Ganesh, S. C. Hawkins, and R. Hiptmair, *Convergence analysis with parameter estimates for a reduced basis acoustic scattering T -matrix method*, IMA J Numer Anal **32** (2012), no. 4, 1348–1374 (en).
8. F. J. García de Abajo, *Colloquium: Light scattering by particle and hole arrays*, Rev. Mod. Phys. **79** (2007), no. 4, 1267–1290.
9. Brendan Gavin, Agnieszka Międlar, and Eric Polizzi, *FEAST eigensolver for nonlinear eigenvalue problems*, Journal of Computational Science **27** (2018), 107–117 (en).
10. R. Guo, M. Nečada, T. K. Hakala, A. I. Väkeväinen, and P. Törmä, *Lasing at \mathbb{S}^2 Points of a Honeycomb Plasmonic Lattice*, Phys. Rev. Lett. **122** (2019), no. 1, 013901.
11. T. K. Hakala, H. T. Rekola, A. I. Väkeväinen, J.-P. Martikainen, M. Nečada, A. J. Moilanen, and P. Törmä, *Lasing in dark and bright modes of a finite-sized plasmonic lattice*, Nature Communications **8** (2017), 13687 (en).
12. Tommi K. Hakala, Antti J. Moilanen, Aaro I. Väkeväinen, Rui Guo, Jani-Petri Martikainen, Konstantinos S. Daskalakis, Heikki T. Rekola, Aleksi Julku, and Päivi Törmä, *Bose–Einstein condensation in a plasmonic lattice*, Nature Phys **14** (2018), no. 7, 739–744 (en).
13. F. S. Ham and B. Segall, *Energy Bands in Periodic Lattices—Green’s Function Method*, Phys. Rev. **124** (1961), no. 6, 1786–1796.
14. Roger F. Harrington, *Field Computation by Moment Methods (IEEE Press Series on Electromagnetic Wave Theory)*, The IEEE PRESS Series in Electromagnetic Waves (Donald G. Dudley, Editor), Wiley-IEEE Press, 1993.
15. Chia Wei Hsu, Bo Zhen, A. Douglas Stone, John D. Joannopoulos, and Marin Soljačić, *Bound states in the continuum*, Nature Reviews Materials **1** (2016), no. 9, 1–13 (en).

16. John David Jackson, *Classical Electrodynamics Third Edition*, 3 edition ed., Wiley, New York, August 1998 (English).
17. Kyoaburo Kambe, *Theory of Electron Diffraction by Crystals*, Zeitschrift für Naturforschung A **22** (1967), no. 4, 422–431.
18. ———, *Theory of Low-Energy Electron Diffraction*, Zeitschrift für Naturforschung A **22** (1967), no. 3, 322–330.
19. ———, *Theory of Low-Energy Electron Diffraction*, Zeitschrift für Naturforschung A **23** (1968), no. 9, 1280–1294.
20. M. Kataja, T. K. Hakala, A. Julku, M. J. Huttunen, S. van Dijken, and P. Törmä, *Surface lattice resonances and magneto-optical response in magnetic nanoparticle arrays*, Nat Commun **6** (2015) (en).
21. Mohammadreza Khorasaninejad and Federico Capasso, *Metalenses: Versatile multifunctional photonic components*, Science **358** (2017), no. 6367 (en).
22. V. G. Kravets, A. V. Kabashin, W. L. Barnes, and A. N. Grigorenko, *Plasmonic Surface Lattice Resonances: A Review of Properties and Applications*, Chem. Rev. **118** (2018), no. 12, 5912–5951.
23. Gerhard Kristensson, *Spherical Vector Waves*, January 2014, Available at <http://www.eit.lth.se/fileadmin/eit/courses/eit080f/Literature/book.pdf>.
24. ———, *Scattering of Electromagnetic Waves by Obstacles*, Scitech Publishing, Edison, NJ, July 2016 (English).
25. Christian Kuttner, *Plasmonics in Sensing: From Colorimetry to SERS Analytics*, Plasmonics (2018) (en).
26. C. Linton, *Lattice Sums for the Helmholtz Equation*, SIAM Rev. **52** (2010), no. 4, 630–674.
27. Pavel Litvinov and Klaus Ziegler, *Rigorous derivation of superposition T-matrix approach from solution of inhomogeneous wave equation*, Journal of Quantitative Spectroscopy and Radiative Transfer **109** (2008), no. 1, 74–88 (en).
28. D. W. Mackowski and M. I. Mishchenko, *A multiple sphere T-matrix Fortran code for use on parallel computer clusters*, Journal of Quantitative Spectroscopy and Radiative Transfer **112** (2011), no. 13, 2182–2192 (en).
29. Daniel W. Mackowski, *MSTM 3.0: A multiple sphere T -matrix FORTRAN code for use on parallel computer clusters*, 2013.
30. Johannes Markkanen, *FastTMM*, 2018, available at https://bitbucket.org/planetarysystemresearch/fastmm_v1.0/.
31. Johannes Markkanen and Alex J. Yuffa, *Fast superposition T-matrix solution for clusters with arbitrarily-shaped constituent particles*, Journal of Quantitative Spectroscopy and Radiative Transfer **189** (2017), 181–188 (en).
32. L. N. Medgyesi-Mitschang, J. M. Putnam, and M. B. Geder, *Generalized method of moments for three-dimensional penetrable scatterers*, J. Opt. Soc. Am. A, JOSAA **11** (1994), no. 4, 1383–1398 (EN).
33. Gustav Mie, *Beiträge zur Optik trüber Medien, speziell kolloidaler Metallösungen*, Ann. Phys. **330** (1908), no. 3, 377–445 (en).
34. Michael I. Mishchenko, Larry D. Travis, and Andrew A. Lacis, *Scattering, Absorption, and Emission of Light by Small Particles*, first ed., Cambridge University Press, 2002.
35. Alexander Moroz, *Quasi-periodic Green's functions of the Helmholtz and Laplace equations*, J. Phys. A: Math. Gen. **39** (2006), no. 36, 11247 (en).
36. Marek Nečada, *QPMS Photonic Multiple Scattering suite*, 2020, source code available at <https://repo.or.cz/qpms.git>.
37. Sara Pourjamal, Tommi K. Hakala, Marek Nečada, Francisco Freire-Fernández, Mikko Kataja, Heikki Rekola, Jani-Petri Martikainen, Päivi Törmä, and Sebastiaan van Dijken, *Lasing in Ni Nanodisk Arrays*, ACS Nano (2019) (en).
38. S. M. Raiyan Kabir, B. M. A. Rahman, and A. Agrawal, *Finite Element Time Domain Method for Photonics*, Recent Trends in Computational Photonics (Arti Agrawal, Trevor Benson, Richard M. De La Rue, and Gregory A. Wurtz, eds.), Springer Series in Optical Sciences, Springer International Publishing, Cham, 2017, pp. 1–37 (en).
39. Aleksandar D. Rakić, Aleksandra B. Djurišić, Jovan M. Elazar, and Marian L. Majewski, *Optical properties of metallic films for vertical-cavity optoelectronic devices*, Appl. Opt., AO **37** (1998), no. 22, 5271–5283 (EN).

40. Mohammad Ramezani, Matthijs Berghuis, and Jaime Gómez Rivas, *Strong light-matter coupling and exciton-polariton condensation in lattices of plasmonic nanoparticles [Invited]*, J. Opt. Soc. Am. B, JOSAB **36** (2019), no. 7, E88–E103 (EN).
41. Mohammad Ramezani, Alexei Halpin, Antonio I. Fernández-Domínguez, Johannes Feist, Said Rahimzadeh-Kalaleh Rodriguez, Francisco J. Garcia-Vidal, and Jaime Gómez Rivas, *Plasmon-exciton-polariton lasing*, Optica, OPTICA **4** (2017), no. 1, 31–37 (EN).
42. Homer Reid, *SCUFF-EM*, 2018.
43. M. T. Homer Reid and Steven G. Johnson, *Efficient Computation of Power, Force, and Torque in BEM Scattering Calculations*, IEEE Transactions on Antennas and Propagation **63** (2015), no. 8, 3588–3598.
44. ScattPort, *Multiple Particle Scattering*, <https://scattport.org/index.php/light-scattering-software/multiple-particle-scattering>, online resource at <https://scattport.org/index.php/light-scattering-software/multiple-particle-scattering>.
45. F. Michael Schulz, Knut Stamnes, and J. J. Stamnes, *Point-group symmetries in electromagnetic scattering*, Journal of the Optical Society of America A **16** (1999), no. 4, 853 (en).
46. N. Stefanou, V. Yannopoulos, and A. Modinos, *Heterostructures of photonic crystals: Frequency bands and transmission coefficients*, Computer Physics Communications **113** (1998), no. 1, 49–77 (en).
47. ———, *MULTTEM 2: A new version of the program for transmission and band-structure calculations of photonic crystals*, Computer Physics Communications **132** (2000), no. 1, 189–196 (en).
48. Dennis M. Sullivan, *Electromagnetic Simulation Using the FDTD Method*, 2 edition ed., Wiley-IEEE Press, Hoboken, New Jersey, June 2013 (English).
49. P. Törmä and W. L. Barnes, *Strong coupling between surface plasmon polaritons and emitters: A review*, Rep. Prog. Phys. **78** (2015), no. 1, 013901 (en).
50. A. I. Väkeväinen, R. J. Moerland, H. T. Rekola, A.-P. Eskelinen, J.-P. Martikainen, D.-H. Kim, and P. Törmä, *Plasmonic Surface Lattice Resonances at the Strong Coupling Regime*, Nano Lett. **14** (2014), no. 4, 1721–1727.
51. Aaro I. Väkeväinen, Antti J. Moilanen, Marek Nečada, Tommi K. Hakala, Konstantinos S. Daskalakis, and Päivi Törmä, *Sub-picosecond thermalization dynamics in condensation of strongly coupled lattice plasmons*, Nature Communications **11** (2020), no. 1, 1–12 (en).
52. Danqing Wang, Weijia Wang, Michael P. Knudson, George C. Schatz, and Teri W. Odom, *Structural Engineering in Plasmon Nanolasers*, Chem. Rev. **118** (2018), no. 6, 2865–2881.
53. Weijia Wang, Mohammad Ramezani, Aaro I. Väkeväinen, Päivi Törmä, Jaime Gómez Rivas, and Teri W. Odom, *The rich photonic world of plasmonic nanoparticle arrays*, Materials Today **21** (2018), no. 3, 303–314.
54. P. C. Waterman, *New Formulation of Acoustic Scattering*, The Journal of the Acoustical Society of America **45** (1969), no. 6, 1417–1429.
55. ———, *Symmetry, Unitarity, and Geometry in Electromagnetic Scattering*, Phys. Rev. D **3** (1971), no. 4, 825–839.
56. Eugene P. Wigner and J. J. Griffin, *Group theory and its application to the quantum mechanics of atomic spectra*, revised ed., Academic Press, 1959.
57. Yu-Lin Xu, *Fortran codes for multi-particle light-scattering calculations*, <https://scattport.org/files/xu/codes.htm>, 2003.
58. Ankun Yang, Thang B. Hoang, Montacer Dridi, Claire Deeb, Maiken H. Mikkelsen, George C. Schatz, and Teri W. Odom, *Real-time tunable lasing from plasmonic nanocavity arrays*, Nat Commun **6** (2015), 6939 (en).
59. LinLin Zhao, K. Lance Kelly, and George C. Schatz, *The Extinction Spectra of Silver Nanoparticle Arrays: Influence of Array Structure on Plasmon Resonance Wavelength and Width†*, J. Phys. Chem. B **107** (2003), no. 30, 7343–7350.
60. Wei Zhou, Montacer Dridi, Jae Yong Suh, Chul Hoon Kim, Dick T. Co, Michael R. Wasielewski, George C. Schatz, and Teri W. Odom, *Lasing action in strongly coupled plasmonic nanocavity arrays*, Nat Nano **8** (2013), no. 7, 506–511 (en).
61. Shengli Zou, Nicolas Janel, and George C. Schatz, *Silver nanoparticle array structures that produce remarkably narrow plasmon lineshapes*, The Journal of Chemical Physics **120** (2004), no. 23, 10871–10875.

8. SUPPLEMENTARY MATERIAL: DERIVATION OF THE 1D AND 2D LATTICE SUMS FOR THE 3D HELMHOLTZ EQUATION WITH GENERAL LATTICE OFFSET

8.1. Periodic Green's functions vs. VSWF lattice sums.

8.1.1. Some definitions and useful relations.

$$\mathcal{H}_l^m(\mathbf{d}) \equiv h_l^+ (|\mathbf{d}|) Y_{l,m}(\hat{\mathbf{d}}),$$

$$\mathcal{J}_l^m(\mathbf{d}) \equiv j_l (|\mathbf{d}|) Y_{l,m}(\hat{\mathbf{d}}).$$

Dual spherical harmonics and waves:

$$\int Y_{l,m} Y'_{l',m'} d\Omega = \delta_{l,l'} \delta_{m,m'},$$

$$\mathcal{J}'^m_l(\mathbf{d}) \equiv j_l (|\mathbf{d}|) Y'_{l,m}(\hat{\mathbf{d}}).$$

Expansion of a plane wave:

$$e^{i\kappa \mathbf{r} \cdot \hat{\mathbf{r}}'} = 4\pi \sum_{l,m} i^n \mathcal{J}'^m_l(\kappa \mathbf{r}) Y_{l,m}(\hat{\mathbf{r}}') = 4\pi \sum_{l,m} i^n \mathcal{J}_l^m(\kappa \mathbf{r}) Y'_{l,m}(\hat{\mathbf{r}}').$$

This one is also convention independent (similarly for \mathcal{H}_l^m):

$$\mathcal{J}_l^m(-\mathbf{r}) = (-1)^l \mathcal{J}_l^m(\mathbf{r}).$$

8.1.2. *Helmholtz equation and Green's functions (in 3D).* Note that the notation does not follow Linton's (where the wavenumbers are often implicit)

$$(\nabla^2 + \kappa^2) G^{(\kappa)}(\mathbf{x}, \mathbf{x}_0) = \delta(\mathbf{x} - \mathbf{x}_0),$$

$$\begin{aligned} G_0^{(\kappa)}(\mathbf{x}, \mathbf{x}_0) &= G_0^{(\kappa)}(\mathbf{x} - \mathbf{x}_0) \\ &= -\frac{e^{i\kappa|\mathbf{x}-\mathbf{x}_0|}}{4\pi|\mathbf{x}-\mathbf{x}_0|} \\ &= -\frac{i\kappa}{4\pi} h_0^+(\kappa|\mathbf{x}-\mathbf{x}_0|) \\ &= -\frac{i\kappa}{\sqrt{4\pi}} \mathcal{H}_0^0(\kappa|\mathbf{x}-\mathbf{x}_0|). \end{aligned}$$

In case of wacky conventions, $G_0^{(\kappa)}(\mathbf{x}, \mathbf{x}_0) = -\frac{i\kappa}{Y_{0,0}} \mathcal{H}_0^0(\kappa|\mathbf{x}-\mathbf{x}_0|)$.

Lattice GF [26, (2.3)]:

$$(8.1) \quad G_\Lambda^{(\kappa)}(\mathbf{s}, \mathbf{k}) \equiv \sum_{\mathbf{R} \in \Lambda} G_0^\kappa(\mathbf{s} - \mathbf{R}) e^{i\mathbf{k} \cdot \mathbf{R}}$$

8.1.3. *GF expansion and lattice sum definition.* Let's define

$$\sigma_l^m(\mathbf{s}, \mathbf{k}) = \sum_{\mathbf{R} \in \Lambda} \mathcal{H}_l^m(\kappa(\mathbf{s} + \mathbf{R})) e^{i\mathbf{k} \cdot \mathbf{R}},$$

and also its dual version

$$\sigma_l'^m(\mathbf{s}, \mathbf{k}) = \sum_{\mathbf{R} \in \Lambda} \mathcal{H}_l'^m(\kappa(\mathbf{s} + \mathbf{R})) e^{i\mathbf{k} \cdot \mathbf{R}}.$$

Inspired by [26, (4.1)]: assuming that $\mathbf{s} \notin \Lambda$, let's expand the lattice Green's function around \mathbf{s} :

$$G_\Lambda^{(\kappa)}(\mathbf{s} + \mathbf{r}, \mathbf{k}) = -i\kappa \sum_{l,m} \tau_l^m(\mathbf{s}, \mathbf{k}) \mathcal{J}_l^m(\kappa \mathbf{r}),$$

and multiply with a dual SH + integrate

$$\begin{aligned} \int d\Omega_{\mathbf{r}} G_\Lambda^{(\kappa)}(\mathbf{s} + \mathbf{r}, \mathbf{k}) Y_{l',m'}'(\hat{\mathbf{r}}) &= -i\kappa \sum_{l,m} \tau_l^m(\mathbf{s}, \mathbf{k}) j_l(\kappa|\mathbf{r}|) \delta_{ll'} \delta_{mm'} \\ (8.2) \qquad \qquad \qquad &= -i\kappa \tau_{l'}^{m'}(\mathbf{s}, \mathbf{k}) j_{l'}(\kappa|\mathbf{r}|). \end{aligned}$$

The expansion coefficients $\tau_l^m(\mathbf{s}, \mathbf{k})$ is then typically extracted by taking the limit $|\mathbf{r}| \rightarrow 0$.

The relation between $\sigma_l^m(\mathbf{s}, \mathbf{k})$ and $\tau_l^m(\mathbf{s}, \mathbf{k})$ can be obtained e.g. from the addition theorem for scalar spherical wavefunctions [26, (C.3)],

$$\mathcal{H}_l^m(\mathbf{a} + \mathbf{b}) = \sum_{l'm'} S_{ll'}^{mm'}(\mathbf{b}) \mathcal{J}_{l'}^{m'}(\mathbf{a}), \quad |\mathbf{a}| < |\mathbf{b}|,$$

where for the zeroth degree and order one has [26, (C.3)]⁵

$$S_{0l'}^{0m'}(\mathbf{b}) = \sqrt{4\pi} \mathcal{H}_{l'}^{m'}(-\mathbf{b}).$$

From the lattice GF definition (8.1)

$$\begin{aligned} G_\Lambda^{(\kappa)}(\mathbf{s} + \mathbf{r}, \mathbf{k}) &\equiv \frac{-i\kappa}{\sqrt{4\pi}} \sum_{\mathbf{R} \in \Lambda} \mathcal{H}_0^0(\kappa(\mathbf{s} + \mathbf{r} - \mathbf{R})) e^{i\mathbf{k} \cdot \mathbf{R}} \\ &= \frac{-i\kappa}{\sqrt{4\pi}} \sum_{\mathbf{R} \in \Lambda} \mathcal{H}_0^0(\kappa(\mathbf{s} + \mathbf{r} - \mathbf{R})) e^{i\mathbf{k} \cdot \mathbf{R}} \\ &= \frac{-i\kappa}{\sqrt{4\pi}} \sum_{\mathbf{R} \in \Lambda} \sum_{l'm'} S_{0l'}^{0m'}(\kappa(\mathbf{s} - \mathbf{R})) \mathcal{J}_{l'}^{m'}(\kappa \mathbf{r}) e^{i\mathbf{k} \cdot \mathbf{R}} \\ &= -i\kappa \sum_{\mathbf{R} \in \Lambda} \sum_{lm} \mathcal{H}_l'^m(-\kappa(\mathbf{s} - \mathbf{R})) \mathcal{J}_l^m(\kappa \mathbf{r}) e^{i\mathbf{k} \cdot \mathbf{R}}, \end{aligned}$$

and mutliplying with a dual SH and integrating

$$\begin{aligned} \int d\Omega_{\mathbf{r}} G_\Lambda^{(\kappa)}(\mathbf{s} + \mathbf{r}, \mathbf{k}) Y_{l',m'}'(\hat{\mathbf{r}}) &= -i\kappa \sum_{\mathbf{R} \in \Lambda} \sum_{lm} \mathcal{H}_l'^m(-\kappa(\mathbf{s} - \mathbf{R})) j_l(\kappa|\mathbf{r}|) \delta_{ll'} \delta_{mm'} e^{i\mathbf{k} \cdot \mathbf{R}} \\ &= -i\kappa \sum_{\mathbf{R} \in \Lambda} \mathcal{H}_{l'}^{m'}(\kappa(-\mathbf{s} + \mathbf{R})) j_{l'}(\kappa|\mathbf{r}|) e^{i\mathbf{k} \cdot \mathbf{R}} \\ &= -i\kappa \sigma_{l'}^{m'}(-\mathbf{s}, \mathbf{k}) j_{l'}(\kappa|\mathbf{r}|), \end{aligned}$$

⁵In a totally convention-independent version probably looks like $S_{0l'}^{0m'}(\mathbf{b}) = Y_{0,0} \mathcal{H}_{l'}^{m'}(-\mathbf{b})$, but the $Y_{0,0}$ will cancel with the expression for GF anyways, so no harm to the final result.

and comparing with (8.2) we have

$$\tau_l^m(\mathbf{s}, \mathbf{k}) = \sigma_l^m(-\mathbf{s}, \mathbf{k}).$$

8.2. Derivation of the 1D and 2D lattice sum. With [26] in hand, the short-range part is rather easy. Let's get the long-range part.

We first need to find the long-range part of the expansion coefficient

$$(8.3) \quad \tau_{l'}^{m'}(\mathbf{s}, \mathbf{k}) = \frac{i}{\kappa j_{l'}(\kappa|\mathbf{r}|)} \int d\Omega_{\mathbf{r}} G_{\Lambda}^{(\kappa)}(\mathbf{s} + \mathbf{r}, \mathbf{k}) Y'_{l', m'}(\hat{\mathbf{r}}).$$

We take [26, (2.24)] with slightly modified notation ($\mathbf{k}_{\mathbf{K}} \equiv \mathbf{K} + \mathbf{k}$)

$$G_{\Lambda}^{(1; \kappa)}(\mathbf{r}) = -\frac{1}{2\pi^{d_c/2} \mathcal{A}} \sum_{\mathbf{K} \in \Lambda^*} e^{i\mathbf{k}_{\mathbf{K}} \cdot \mathbf{r}} \int_{1/\eta}^{\infty} e^{i\pi/4} e^{-\kappa^2 \gamma^2 t^2/4} e^{-|\mathbf{r}^\perp|^2/t^2} t^{1-d_c} dt$$

or, evaluated at point $\mathbf{s} + \mathbf{r}$ instead

$$G_{\Lambda}^{(1; \kappa)}(\mathbf{s} + \mathbf{r}) = -\frac{1}{2\pi^{d_c/2} \mathcal{A}} \sum_{\mathbf{K} \in \Lambda^*} e^{i\mathbf{k}_{\mathbf{K}} \cdot (\mathbf{s} + \mathbf{r})} \int_{1/\eta}^{\infty} e^{i\pi/4} e^{-\kappa^2 \gamma^2 t^2/4} e^{-|\mathbf{s}^\perp + \mathbf{r}^\perp|^2/t^2} t^{1-d_c} dt.$$

The integral can be by substitutions taken into the form

$$G_{\Lambda}^{(1; \kappa)}(\mathbf{s} + \mathbf{r}) = -\frac{1}{2\pi^{d_c/2} \mathcal{A}} \sum_{\mathbf{K} \in \Lambda^*} e^{i\mathbf{k}_{\mathbf{K}} \cdot (\mathbf{s} + \mathbf{r})} \int_{\kappa^2 \gamma_m^2/4\eta^2}^{\infty \exp(i\pi/2)} e^{-\tau} e^{-|\mathbf{s}_\perp + \mathbf{r}_\perp|^2 \kappa^2 \gamma_m^2/4\tau} \tau^{-\frac{d_c}{2}} d\tau.$$

Let's do the integration to get $\tau_l^m(\mathbf{s}, \mathbf{k})$

$$\begin{aligned} \int d\Omega_{\mathbf{r}} G_{\Lambda}^{(1; \kappa)}(\mathbf{s} + \mathbf{r}) Y'_{l', m'}(\hat{\mathbf{r}}) &= -\frac{1}{2\pi^{d_c/2} \mathcal{A}} \int d\Omega_{\mathbf{r}} Y'_{l', m'}(\hat{\mathbf{r}}) \sum_{\mathbf{K} \in \Lambda^*} e^{i\mathbf{k}_{\mathbf{K}} \cdot (\mathbf{s} + \mathbf{r})} \times \\ &\times \int_{\kappa^2 \gamma_{\mathbf{K}}^2/4\eta^2}^{\infty \exp(i\pi/2)} e^{-\tau} e^{-|\mathbf{s}_\perp + \mathbf{r}_\perp|^2 \kappa^2 \gamma_{\mathbf{K}}^2/4\tau} \tau^{-\frac{d_c}{2}} d\tau. \end{aligned}$$

The \mathbf{r} -dependent plane wave factor can be also written as

$$\begin{aligned} e^{i\mathbf{k}_{\mathbf{K}} \cdot \mathbf{r}} &= e^{i|\mathbf{k}_{\mathbf{K}}| |\mathbf{r}| \hat{\mathbf{k}}_{\mathbf{K}} \cdot \hat{\mathbf{r}}} = 4\pi \sum_{lm} i^l \mathcal{J}'_l{}^m(|\mathbf{k}_{\mathbf{K}}| |\mathbf{r}|) Y_{l, m}(\hat{\mathbf{k}}_{\mathbf{K}}) \\ &= 4\pi \sum_{lm} i^l j_l(|\mathbf{k}_{\mathbf{K}}| |\mathbf{r}|) Y'_{l, m}(\hat{\mathbf{r}}) Y_{l, m}(\hat{\mathbf{k}}_{\mathbf{K}}), \end{aligned}$$

so

$$\begin{aligned} \int d\Omega_{\mathbf{r}} G_{\Lambda}^{(1; \kappa)}(\mathbf{s} + \mathbf{r}) Y'_{l', m'}(\hat{\mathbf{r}}) &= -\frac{1}{2\pi^{d_c/2} \mathcal{A}} \int d\Omega_{\mathbf{r}} Y'_{l', m'}(\hat{\mathbf{r}}) \frac{1}{2\pi \mathcal{A}} \times \\ &\times \sum_{\mathbf{K} \in \Lambda^*} e^{i\mathbf{k}_{\mathbf{K}} \cdot \mathbf{s}} \sum_{lm} 4\pi i^l j_l(|\mathbf{k}_{\mathbf{K}}| |\mathbf{r}|) Y'_{l, m}(\hat{\mathbf{r}}) Y_{l, m}(\hat{\mathbf{k}}_{\mathbf{K}}) \times \\ &\times \int_{\kappa^2 \gamma_{\mathbf{K}}^2/4\eta^2}^{\infty \exp(i\pi/2)} e^{-\tau} e^{-|\mathbf{s}_\perp + \mathbf{r}_\perp|^2 \kappa^2 \gamma_{\mathbf{K}}^2/4\tau} \tau^{-\frac{d_c}{2}} d\tau. \end{aligned}$$

We also have

$$\begin{aligned} e^{-|\mathbf{s}_\perp + \mathbf{r}_\perp|^2 \kappa^2 \gamma_{\mathbf{K}}^2 / 4\tau} &= e^{-(|\mathbf{s}_\perp|^2 + |\mathbf{r}_\perp|^2 + 2\mathbf{r}_\perp \cdot \mathbf{s}_\perp) \kappa^2 \gamma_{\mathbf{K}}^2 / 4\tau} \\ &= e^{-|\mathbf{s}_\perp|^2 \kappa^2 \gamma_{\mathbf{K}}^2 / 4\tau} \sum_{j=0}^{\infty} \frac{1}{j!} \left(-\frac{(|\mathbf{r}_\perp|^2 + 2\mathbf{r}_\perp \cdot \mathbf{s}_\perp) \kappa^2 \gamma_{\mathbf{K}}^2}{4\tau} \right)^j, \end{aligned}$$

hence

$$\begin{aligned} \int d\Omega_{\mathbf{r}} G_{\Lambda}^{(1;\kappa)}(\mathbf{s} + \mathbf{r}) Y'_{l',m'}(\hat{\mathbf{r}}) &= -\frac{1}{2\pi^{d_c/2} \mathcal{A}} \int d\Omega_{\mathbf{r}} Y'_{l',m'}(\hat{\mathbf{r}}) \sum_{\mathbf{K} \in \Lambda^*} e^{i\mathbf{K} \cdot \mathbf{s}} \times \\ &\quad \times \sum_{lm} 4\pi i^l j_l(|\mathbf{K}| |\mathbf{r}|) Y'_{l,m}(\hat{\mathbf{r}}) Y_{l,m}(\hat{\mathbf{K}}_{\mathbf{K}}) \times \\ &\quad \times \sum_{j=0}^{\infty} \frac{1}{j!} \left(-\frac{(|\mathbf{r}_\perp|^2 + 2\mathbf{r}_\perp \cdot \mathbf{s}_\perp) \kappa^2 \gamma_{\mathbf{K}}^2}{4} \right)^j \times \\ &\quad \times \underbrace{\int_{\kappa^2 \gamma_{\mathbf{K}}^2 / 4\eta^2}^{\infty \exp(i\pi/2)} e^{-\tau} e^{-|\mathbf{s}_\perp|^2 \kappa^2 \gamma_{\mathbf{K}}^2 / 4\tau} \tau^{-\frac{d_c}{2} - j} d\tau}_{\Delta_j^{(d_\Lambda)}} \\ &= -\frac{1}{2\pi^{d_c/2} \mathcal{A}} \sum_{\mathbf{K} \in \Lambda^*} e^{i\mathbf{K} \cdot \mathbf{s}} \sum_{lm} 4\pi i^l j_l(|\mathbf{K}| |\mathbf{r}|) Y_{l,m}(\hat{\mathbf{K}}_{\mathbf{K}}) \sum_{j=0}^{\infty} \frac{\Delta_j^{(d_\Lambda)}}{j!} \times \\ &\quad \times \int d\Omega_{\mathbf{r}} Y'_{l',m'}(\hat{\mathbf{r}}) Y'_{l,m}(\hat{\mathbf{r}}) \left(-\frac{(|\mathbf{r}_\perp|^2 + 2\mathbf{r}_\perp \cdot \mathbf{s}_\perp) \kappa^2 \gamma_{\mathbf{K}}^2}{4} \right)^j \\ &= -\frac{1}{2\pi^{d_c/2} \mathcal{A}} \sum_{\mathbf{K} \in \Lambda^*} e^{i\mathbf{K} \cdot \mathbf{s}} \sum_{lm} 4\pi i^l j_l(|\mathbf{K}| |\mathbf{r}|) Y_{l,m}(\hat{\mathbf{K}}_{\mathbf{K}}) \sum_{j=0}^{\infty} \frac{(-1)^j}{j!} \Delta_j^{(d_\Lambda)} \times \\ &\quad \times \left(\frac{\kappa \gamma_{\mathbf{K}}}{2} \right)^{2j} \sum_{k=0}^j \int d\Omega_{\mathbf{r}} Y'_{l',m'}(\hat{\mathbf{r}}) Y'_{l,m}(\hat{\mathbf{r}}) |\mathbf{r}_\perp|^{2(j-k)} (2\mathbf{r}_\perp \cdot \mathbf{s}_\perp)^k. \end{aligned}$$

The integral $\Delta_j^{(d_\Lambda)}$ is (for the 2D case) equivalent to that in [19].

If we label $|\mathbf{r}_\perp| |\mathbf{s}_\perp| \cos \varphi \equiv \mathbf{r}_\perp \cdot \mathbf{s}_\perp$, we have

$$\begin{aligned} \int d\Omega_{\mathbf{r}} G_{\Lambda}^{(1;\kappa)}(\mathbf{s} + \mathbf{r}) Y'_{l',m'}(\hat{\mathbf{r}}) &= -\frac{1}{2\pi^{d_c/2} \mathcal{A}} \sum_{\mathbf{K} \in \Lambda^*} e^{i\mathbf{K} \cdot \mathbf{s}} \sum_{lm} 4\pi i^l j_l(|\mathbf{K}| |\mathbf{r}|) Y_{l,m}(\hat{\mathbf{K}}_{\mathbf{K}}) \times \\ &\quad \times \sum_{j=0}^{\infty} \frac{(-1)^j}{j!} \Delta_j^{(d_\Lambda)} \left(\frac{\kappa \gamma_{\mathbf{K}}}{2} \right)^{2j} \sum_{k=0}^j (2|\mathbf{s}_\perp|)^k \int d\Omega_{\mathbf{r}} Y'_{l',m'}(\hat{\mathbf{r}}) Y'_{l,m}(\hat{\mathbf{r}}) |\mathbf{r}_\perp|^{2j-k} (\cos \varphi)^k, \end{aligned}$$

and if we label $|\mathbf{r}| \sin \vartheta \equiv |\mathbf{r}_\perp|$

$$\begin{aligned} \int d\Omega_{\mathbf{r}} G_{\Lambda}^{(1;\kappa)}(\mathbf{s} + \mathbf{r}) Y'_{l',m'}(\hat{\mathbf{r}}) &= -\frac{1}{2\pi^{d_c/2} \mathcal{A}} \sum_{\mathbf{K} \in \Lambda^*} e^{i\mathbf{K}\mathbf{K} \cdot \mathbf{s}} \times \\ &\times \sum_{lm} 4\pi i^l j_l(|\mathbf{K}\mathbf{K}| |\mathbf{r}|) Y_{l,m}(\hat{\mathbf{K}}) \sum_{j=0}^{\infty} \frac{(-1)^j}{j!} \Delta_j^{(d_\Lambda)} \left(\frac{\kappa \gamma_{\mathbf{K}\mathbf{K}}}{2} \right)^{2j} \times \\ &\times \sum_{k=0}^j |\mathbf{r}|^{2j-k} (2|\mathbf{s}_\perp|)^k \int d\Omega_{\mathbf{r}} Y'_{l',m'}(\hat{\mathbf{r}}) Y'_{l,m}(\hat{\mathbf{r}}) (\sin \vartheta)^{2j-k} (\cos \varphi)^k. \end{aligned}$$

Now let's put the RHS into (8.3) and try eliminating some sum by taking the limit $|\mathbf{r}| \rightarrow 0$. We have $j_l(|\mathbf{K}\mathbf{K}| |\mathbf{r}|) \sim (|\mathbf{K}\mathbf{K}| |\mathbf{r}|)^l / (2l+1)!!$; the denominator from (8.3) behaves like $j_{l'}(\kappa |\mathbf{r}|) \sim (\kappa |\mathbf{r}|)^{l'} / (2l'+1)!!$. The leading terms are hence those with $|\mathbf{r}|^{l-l'+2j-k}$. So

$$\begin{aligned} \tau_{l'}^{m'}(\mathbf{s}, \mathbf{k}) &= \frac{-i}{2\pi^{d_c/2} \mathcal{A} \kappa^{1+l'}} (2l'+1)!! \sum_{\mathbf{K} \in \Lambda^*} e^{i\mathbf{K}\mathbf{K} \cdot \mathbf{s}} \sum_{lm} 4\pi i^l \frac{|\mathbf{K}\mathbf{K}|^l}{(2l+1)!!} Y_{l,m}(\hat{\mathbf{K}}) \times \\ &\times \sum_{j=0}^{\infty} \frac{(-1)^j}{j!} \Delta_j^{(d_\Lambda)} \left(\frac{\kappa \gamma_{\mathbf{K}\mathbf{K}}}{2} \right)^{2j} \sum_{k=0}^j \delta_{l'-l, 2j-k} (2|\mathbf{s}_\perp|)^k \times \\ &\times \int d\Omega_{\mathbf{r}} Y'_{l',m'}(\hat{\mathbf{r}}) Y'_{l,m}(\hat{\mathbf{r}}) (\sin \vartheta)^{l'-l} (\cos \varphi)^k. \end{aligned}$$

Let's now focus on rearranging the sums; we have

$$S(l') \equiv \sum_{l=0}^{\infty} \sum_{j=0}^{\infty} \sum_{k=0}^j \delta_{l'-l, 2j-k} f(l', l, j, k) = \sum_{l=0}^{\infty} \sum_{j=0}^{\infty} \sum_{k=0}^j \delta_{l'-l, 2j-k} f(l', l, j, 2j-l'+l).$$

We have $0 \leq k \leq j$, hence $0 \leq 2j-l'+l \leq j$, hence $-2j \leq -l'+l \leq -j$, hence also $l'-2j \leq l \leq l'-j$, which gives the opportunity to swap the l, j sums and the l -sum becomes finite; so also consuming $\sum_{k=0}^j \delta_{l'-l, 2j-k}$ we get

$$S(l') = \sum_{j=0}^{\infty} \sum_{l=\max(0, l'-2j)}^{l'-j} f(l', l, j, 2j-l'+l).$$

Finally, we see that the interval of valid l becomes empty when $l'-j < 0$, i.e. $j > l'$; so we get a finite sum

$$S(l') = \sum_{j=0}^{l'} \sum_{l=\max(0, l'-2j)}^{l'-j} f(l', l, j, 2j-l'+l).$$

Applying rearrangement,

$$\begin{aligned} \tau_{l'}^{m'}(\mathbf{s}, \mathbf{k}) &= \frac{-i}{2\pi^{d_c/2} \mathcal{A}\kappa} \frac{(2l'+1)!!}{\kappa^{l'}} \sum_{\mathbf{K} \in \Lambda^*} e^{i\mathbf{k}\mathbf{K} \cdot \mathbf{s}} \sum_{j=0}^{l'} \frac{(-1)^j}{j!} \Delta_j^{(d_\Lambda)} \left(\frac{\kappa\gamma\mathbf{k}\mathbf{K}}{2} \right)^{2j} \times \\ &\quad \times \sum_{l=\max(0, l'-2j)}^{l'-j} 4\pi i^l (2|\mathbf{s}_\perp|)^{2j-l'+l} \frac{|\mathbf{k}\mathbf{K}|^l}{(2l+1)!!} \times \\ &\quad \times \sum_{m=-l}^l Y_{l,m}(\hat{\mathbf{k}}\mathbf{K}) \int d\Omega_{\mathbf{r}} Y'_{l',m'}(\hat{\mathbf{r}}) Y'_{l,m}(\hat{\mathbf{r}}) (\sin \vartheta)^{l'-l} (\cos \varphi)^{2j-l'+l}, \end{aligned}$$

or replacing the angles with their original definition,

$$\begin{aligned} \tau_{l'}^{m'}(\mathbf{s}, \mathbf{k}) &= \frac{-i}{2\pi^{d_c/2} \mathcal{A}\kappa} \frac{(2l'+1)!!}{\kappa^{l'}} \sum_{\mathbf{K} \in \Lambda^*} e^{i\mathbf{k}\mathbf{K} \cdot \mathbf{s}} \sum_{j=0}^{l'} \frac{(-1)^j}{j!} \Delta_j^{(d_\Lambda)} \left(\frac{\kappa\gamma\mathbf{K}}{2} \right)^{2j} \times \\ &\quad \times \sum_{l=\max(0, l'-2j)}^{l'-j} 4\pi i^l (2|\mathbf{s}_\perp|)^{2j-l'+l} \frac{|\mathbf{k}\mathbf{K}|^l}{(2l+1)!!} \\ &\quad \times \sum_{m=-l}^l Y_{l,m}(\hat{\mathbf{K}}) \int d\Omega_{\mathbf{r}} Y'_{l',m'}(\hat{\mathbf{r}}) Y'_{l,m}(\hat{\mathbf{r}}) \left(\frac{|\mathbf{r}_\perp|}{|\mathbf{r}|} \right)^{l'-l} \left(\frac{\mathbf{r}_\perp \cdot \mathbf{s}_\perp}{|\mathbf{r}_\perp| |\mathbf{s}_\perp|} \right)^{2j-l'+l}, \end{aligned}$$

and if we want a $\sigma_{l'}^{m'}(\mathbf{s}, \mathbf{k})$ instead, we reverse the sign of \mathbf{s} and replace all spherical harmonics with their dual counterparts:

$$\begin{aligned} \sigma_{l'}^{m'}(\mathbf{s}, \mathbf{k}) &= \frac{-i}{2\pi^{d_c/2} \mathcal{A}\kappa} \frac{(2l'+1)!!}{\kappa^{l'}} \sum_{\mathbf{K} \in \Lambda^*} e^{-i\mathbf{k}\mathbf{K} \cdot \mathbf{s}} \sum_{j=0}^{l'} \frac{(-1)^j}{j!} \Delta_j^{(d_\Lambda)} \left(\frac{\kappa\gamma\mathbf{k}\mathbf{K}}{2} \right)^{2j} \times \\ &\quad \times \sum_{l=\max(0, l'-2j)}^{l'-j} 4\pi i^l (2|\mathbf{s}_\perp|)^{2j-l'+l} \frac{|\mathbf{k}\mathbf{K}|^l}{(2l+1)!!} \times \\ &\quad \times \sum_{m=-l}^l Y'_{l,m}(\hat{\mathbf{k}}\mathbf{K}) \int d\Omega_{\mathbf{r}} Y_{l',m'}(\hat{\mathbf{r}}) Y_{l,m}(\hat{\mathbf{r}}) \left(\frac{|\mathbf{r}_\perp|}{|\mathbf{r}|} \right)^{l'-l} \left(\frac{-\mathbf{r}_\perp \cdot \mathbf{s}_\perp}{|\mathbf{r}_\perp| |\mathbf{s}_\perp|} \right)^{2j-l'+l}, \end{aligned}$$

and remembering that in the plane wave expansion the “duality” is interchangeable,

$$\begin{aligned} \sigma_{l'}^{m'}(\mathbf{s}, \mathbf{k}) &= \frac{-i}{2\pi^{d_c/2} \mathcal{A}\kappa} \frac{(2l'+1)!!}{\kappa^{l'}} \sum_{\mathbf{K} \in \Lambda^*} e^{-i\mathbf{k}\mathbf{K} \cdot \mathbf{s}} \sum_{j=0}^{l'} \frac{(-1)^j}{j!} \Delta_j^{(d_\Lambda)} \left(\frac{\kappa\gamma\mathbf{k}\mathbf{K}}{2} \right)^{2j} \times \\ &\quad \times \sum_{l=\max(0, l'-2j)}^{l'-j} 4\pi i^l (2|\mathbf{s}_\perp|)^{2j-l'+l} \frac{|\mathbf{k}\mathbf{K}|^l}{(2l+1)!!} \times \\ &\quad \times \sum_{m=-l}^l Y_{l,m}(\hat{\mathbf{k}}\mathbf{K}) \underbrace{\int d\Omega_{\mathbf{r}} Y_{l',m'}(\hat{\mathbf{r}}) Y_{l,m}(\hat{\mathbf{r}}) \left(\frac{|\mathbf{r}_\perp|}{|\mathbf{r}|} \right)^{l'-l} \left(\frac{-\mathbf{r}_\perp \cdot \mathbf{s}_\perp}{|\mathbf{r}_\perp| |\mathbf{s}_\perp|} \right)^{2j-l'+l}}_{\equiv A_{l',l,m',m,j}^{(d_\Lambda)}}. \end{aligned}$$

The angular integral is easier to evaluate when $d_\Lambda = 2$, because then \mathbf{r}_\perp is parallel (or antiparallel) to \mathbf{s}_\perp , which gives

$$A_{l',l,m',m,j}^{(2)} = \left(-\frac{\mathbf{r}_\perp \cdot \mathbf{s}_\perp}{|\mathbf{r}_\perp \cdot \mathbf{s}_\perp|} \right)^{2j-l'+l} \int d\Omega_{\mathbf{r}} Y_{l',m'}(\hat{\mathbf{r}}) Y_{l,m}'(\hat{\mathbf{r}}) \left(\frac{|\mathbf{r}_\perp|}{|\mathbf{r}|} \right)^{2j}$$

and if we set the normal of the lattice correspond to the z axis, the azimuthal part of the integral will become zero unless $m' = m$ for any meaningful spherical harmonics convention, and the polar part for the only nonzero case has a closed-form expression, see e.g. [26, (A.15)], so one arrives at an expression similar to [19, (3.15)]

$$(8.4) \quad \sigma_{l,m}^{(L,\eta)}(\mathbf{k}, \mathbf{s}) = -\frac{i^{l+1}}{\kappa^2 \mathcal{A}} \pi^{3/2} 2^{((l-m)/2)!((l+m)/2)!} \times \\ \times \sum_{\mathbf{K} \in \Lambda^*} e^{i\mathbf{k}\mathbf{K} \cdot \mathbf{s}} Y_{l,m}(\mathbf{k}\mathbf{K}) \sum_{j=0}^{l-|m|} (-1)^j \gamma_{\mathbf{k}\mathbf{K}}^2 2^{j+1} \times \\ \times \Delta_j \left(\frac{\kappa^2 \gamma_{\mathbf{k}\mathbf{K}}^2}{4\eta^2}, -i\kappa \gamma_{\mathbf{k}\mathbf{K}}^2 s_\perp \right) \times \\ \times \sum_{\substack{j \leq s \leq \min(2j, l-|m|) \\ l-j+|m| \text{ even}}} \frac{1}{(2j-s)!(s-j)!} \frac{(-\kappa s_\perp)^{2j-s} (|\mathbf{k}\mathbf{K}|/\kappa)^{l-s}}{\left(\frac{1}{2}(l-m-s)\right)! \left(\frac{1}{2}(l+m-s)\right)!}$$

where $s_\perp \equiv \mathbf{s} \cdot \hat{\mathbf{z}} = \mathbf{s}_\perp \cdot \hat{\mathbf{z}}$. If $d_\Lambda = 1$, the angular becomes more complicated to evaluate due to the different behaviour of the $\mathbf{r}_\perp \cdot \mathbf{s}_\perp / |\mathbf{r}_\perp| |\mathbf{s}_\perp|$ factor. The choice of coordinates can make most of the terms disappear: if the lattice is set parallel to the z axis, $A_{l',l,m',m,j}^{(1)}$ is zero unless $m = 0$, but one still has

$$A_{l',l,m',0,j}^{(1)} = \pi \delta_{m',l'-l-2j} \lambda'_{l0} \lambda_{l'm'} \int_{-1}^1 dx P_{l'}^{m'}(x) P_l^0(x) (1-x^2)^{\frac{l'-l}{2}}$$

where λ_{lm} are constants depending on the conventions for spherical harmonics. This does not seem to have such a nice closed-form expression as in the 2D case, but it can be evaluated e.g. using the common recurrence relations for associated Legendre polynomials. Of course when $\mathbf{s} = 0$, one gets relatively nice closed expressions, such as those in [26].